Received: Added at production | Revised: Added at production | Accepted: Added at production

DOI: xxx/xxxx

ARTICLE TYPE

Tracking Amplitude Extrema of Nonlinear Frequency Responses using the Harmonic Balance Method†

Ghislain Raze* | Martin Volvert | Gaetan Kerschen

[1]Space Structures and Systems Laboratory, Aerospace and Mechanical Engineering Department, University of Liège, Belgium

Correspondence
*Ghislain Raze, Space Structures and Systems Laboratory, Aerospace and Mechanical Engineering Department, University of Liège
Quartier Polytech 1 (B52/3), Allée de la Découverte 9, B-4000 Liège, Belgium.
Email: g.raze@uliege.be

Summary

This work proposes a novel efficient method to track the evolution of amplitude extrema featured by frequency responses of nonlinear systems using the harmonic balance method. Means to compute the amplitude of a Fourier series are first outlined, and a set of equations characterizing a local extremum of a nonlinear frequency response amplitude curve is derived. Efficient numerical procedures are used to evaluate these equations and their derivatives (including second-order ones) to embed them in a predictor-corrector continuation framework. The proposed approach is illustrated on three examples of increasing complexity, namely a Helmholtz-Duffing oscillator, a two-degree-of-freedom system with a modal interaction, and a doubly clamped von Kàrmàn beam with a nonlinear tuned vibration absorber.

KEYWORDS:
Amplitude Resonance, Extremum Tracking, Harmonic Balance, Companion Matrix, Bordered System, Alternating Frequency-Time

1 | INTRODUCTION

The vibration analysis of nonlinear structural systems is of crucial interest to academia and industry. An extensive amount of work has been carried out to provide strong theoretical [1,2], numerical [3,4] and experimental [5] foundations to the field. Robust tools now exist to compute the response of nonlinear systems to different excitations, but remain to this day rather numerically expensive owing to the large dimensionality and nonlinearity of most systems of interest.

The last decades have witnessed a growing interest in the intentional use of nonlinearity, which has proven beneficial in a number of cases. An important research avenue is the field of nonlinear vibration mitigation. Several solutions, such as nonlinear energy sinks [6,7], autoparametric vibration absorbers [8,9], nonlinear tuned vibration absorbers [10,11], friction devices [12,13] and impact dampers [14,15,16] have demonstrated beneficial strengths over traditional linear solutions. Another, more recent trend consists in adding nonlinear elements to a nonlinear structure in order to prescribe its characteristics, e.g., by linearizing its global behavior. Examples include tailoring the bias voltage of electrostatic microresonators for response linearization [17], optimizing normal form coefficients [18] and linearizing resonances [19,20].

Computational tools are extensively used to assess nonlinear responses and to verify nonlinear designs. A number of open-source software are able to solve the nonlinear equations at hand using, for instance, a shooting procedure [3,21], orthogonal collocation [22,23,24,25] or the harmonic balance (HB) method [4,26,27]. Bifurcation tracking [28,29,30] can provide great insight into the

†Tracking Amplitude Extrema of Nonlinear Frequency Responses using the Harmonic Balance Method
Abbreviations: AFT, alternating frequency-time; DoF, degree of freedom; HB, harmonic balance; NFR, nonlinear frequency response; NLTVA, nonlinear tuned vibration absorber

behavior of a nonlinear system with relatively limited effort. For instance, it was used as a means to characterize internal resonances[31] and to improve vibration absorbers designs[32]. A multiparametric recursive version allowed to control highly nonlinear phenomena such as the occurrence of an isolated response[33].

A typical quantity of engineering interest is the maximum amplitude that can be undergone by some degrees of freedom (DoFs) of a structure under specific loading scenarios, and can be a performance measure in vibration mitigation. Robust algorithms have been developed to find the global maximum amplitude for the response of linear systems[34,35]. This question is still an open challenge for nonlinear systems. Petrov[36] was the first to propose a numerical method that allowed to track the amplitude resonance of a single harmonic for bladed discs subjected to friction. Liao and Sun[37] cast the problem to an optimization one and used a multistart gradient-based optimizer to find the worst-case maximum amplitude. Renault et al[38] proposed a method resembling bifurcation tracking and able to follow the single-harmonic amplitude resonances (and antiresonances) of nonlinear frequency responses. Förster and Krack[39] introduced an alternative phase resonance-based approach for primary resonances, with the underlying assumption that amplitude resonance occurs for a fixed value of the phase lag, typically close to quadrature. They illustrated the computational interest of this method for several lightly-damped examples. This approach is relatively easily experimentally implemented if phase quadrature is sought[40,41,42]. The relevance of phase resonance for nonlinear modal analysis was rigorously proven for weakly forced and damped structures[43]. Specific phase relations were also shown to characterize the non-primary resonances of a Duffing oscillator[44,45].

The extrema of a curve can be mathematically defined as the point at which the derivative of the curve with respect to a bifurcation parameter is equal to zero. First derivatives thus typically appear in the nonlinear equations characterizing the extrema. Newton-based methods are generally used to solve these equations and require their derivatives, and therefore second-order derivatives of the problem at hand are involved. Bifurcation tracking algorithms work with the eigenvalues of the Jacobian matrix in the characterizing equations and thus typically have similar requirements. These second-order derivatives are often deemed complicated to obtain[4]. State-of-the-art methods typically resort to finite differences[3,28,29,30,46] or in some cases include the full computation of the third-order tensor of second derivatives[46,47,48]. Automatic differentiation[4,49] constitutes another interesting approach but is seldom used.

None of the aforementioned works provides a method able to efficiently and consistently track multi-harmonic amplitude resonances, or, more generally, the local extrema of nonlinear frequency response amplitude of the displacement, velocity or acceleration of arbitrary nonlinear systems. A first purpose of the present work is to fill this gap using the HB method. Such an extremum tracking procedure can deal with arbitrarily high damping and with highly multi-harmonic responses, such as non-primary resonances and acceleration responses in general. As stated in[39], this approach requires second-order derivatives, which can be cumbersome to compute. A second contribution of this work is thus to propose an efficient method to compute the second-order derivatives of smooth nonlinearities based on the alternating frequency-time (AFT) approach[50]. This method neither resorts to finite differences nor requires the explicit computation and storage of third-order tensors. However, it requires the analytical knowledge of the second derivatives of the functional forms of the nonlinearities.

This work is organized as follows. Section 2 first reviews the basic features of the HB method and means to compute the multi-harmonic amplitude of periodic solutions described by their Fourier series. Section 3 then introduces the equations characterizing the extrema of the nonlinear frequency response amplitude based on a generalization of the formulation used in[38]. The equations are solved using a predictor-corrector continuation scheme, and the computation of the necessary derivatives is presented. In particular, a strategy to compute second-order derivatives is proposed in Section 4. Section 5 discusses additional numerical features, namely stability assessment and computational complexity. Section 6 finally illustrates the proposed method with several examples, namely a Helmholtz-Duffing oscillator, a two-DoF system, and a doubly clamped beam.

2 | NONLINEAR FREQUENCY RESPONSE

A nonlinear system governed by the following second-order ordinary differential equations

$$\mathbf{M}\ddot{\mathbf{x}}(t) + \mathbf{C}\dot{\mathbf{x}}(t) + \mathbf{K}\mathbf{x}(t) + \mathbf{f}_{\text{nl}}(\mathbf{x}(t), \dot{\mathbf{x}}(t), t) = \lambda \mathbf{f}_{\text{ext}}(t) \tag{1}$$

is considered, where $\mathbf{M}$, $\mathbf{C}$ and $\mathbf{K}$ are the structural mass, damping and stiffness matrices, respectively, $\mathbf{x}$ is the vector of generalized DoFs, and $\mathbf{f}_{\text{ext}}$ and $\mathbf{f}_{\text{nl}}$ are the associated generalized loading vectors related to the external and nonlinear and/or parametric forces, respectively. λ is a parameter used to describe the amplitude of the external forcing, and an overdot denotes derivation with respect to time (t).

2.1 | Harmonic balance formalism

To compute the periodic solutions of Equation (1) under a periodic external (or parametric) forcing, a classical HB formalism is used[4,29]. $\mathbf{x}$ is accordingly expressed as a truncated Fourier series using a vector of harmonic coefficients $\mathbf{z}$

$$\mathbf{x}(t) = (\mathbf{Q}(\omega t) \otimes \mathbf{I})\,\mathbf{z}, \tag{2}$$

where ω is the fundamental angular frequency of motion (of which the external and parametric forcing frequencies are integer multiples), $\mathbf{Q}(\omega t)$ is a vector of $2N_h + 1$ harmonic functions[‡]

$$\mathbf{Q}(\omega t) = \left[\frac{1}{\sqrt{2}}\ \sin(\omega t)\ \cos(\omega t)\ \cdots\ \sin(N_h\omega t)\ \cos(N_h\omega t)\right], \tag{3}$$

$\mathbf{I}$ is the identity matrix, and $\otimes$ denotes the Kronecker product. If $\mathbf{x}$ is a column vector of length N_x, then $\mathbf{z}$ is a column vector of length $N_z = (2N_h + 1)N_x$. Using a Galerkin procedure, Equation (1) may be expressed in the frequency domain as a set of N_z nonlinear algebraic equations

$$\mathbf{A}(\omega)\mathbf{z} + \mathbf{b}(\mathbf{z}, \omega) = \lambda\mathbf{b}_{\text{ext}}, \tag{4}$$

where the matrix $\mathbf{A}$ is associated to the linear forces and is given by

$$\mathbf{A}(\omega) = \omega^2\boldsymbol{\nabla}^2 \otimes \mathbf{M} + \omega\boldsymbol{\nabla} \otimes \mathbf{C} + \mathbf{I} \otimes \mathbf{K} \tag{5}$$

with the frequency-normalized differential operator

$$\boldsymbol{\nabla} = \begin{bmatrix} 0 & & \mathbf{0} \\ & \begin{bmatrix} 1 & 0 & \cdots & 0 \\ 0 & 2 & \cdots & 0 \\ \vdots & \vdots & \ddots & \vdots \\ 0 & 0 & \cdots & N_h \end{bmatrix} \otimes \begin{bmatrix} 0 & -1 \\ 1 & 0 \end{bmatrix} & \\ \mathbf{0} & & \end{bmatrix}. \tag{6}$$

$\mathbf{b}$ and $\mathbf{b}_{\text{ext}}$ may be obtained using an AFT procedure[50] (see Section 3.3.1), although the latter can also be given directly. Once these terms are determined, Equation (4) can be solved for $\mathbf{z}$ using, e.g., a Newton-Raphson procedure. The full details to derive the above HB equations with this formalism are given in[29].

2.2 | Nonlinear frequency response amplitude

We now focus on a representation of the response of the nonlinear system defined by Equation (1) for an arbitrary time-dependent DoF u of interest, and in particular, on the amplitude of its nonlinear frequency response (NFR). This DoF is assumed to be obtained from the r^{th} time derivative of $\mathbf{x}$ using a localization vector $\mathbf{w}_u$ of length N_x as

$$u(t) = \mathbf{w}_u^T \frac{d^r\mathbf{x}(t)}{dt^r} = \mathbf{w}_u^T\,(\mathbf{Q}(\omega t)\omega^r\boldsymbol{\nabla}^r \otimes \mathbf{I})\,\mathbf{z}, \tag{7}$$

where superscript T denotes a transposition. Typical values of r are $r = 0$, 1 and 2 for the displacement, velocity and acceleration, respectively. Using twice a basic identity of the Kronecker product $(\mathbf{S} \otimes \mathbf{U})(\mathbf{T} \otimes \mathbf{V}) = (\mathbf{ST}) \otimes (\mathbf{UV})$ for matrices of compatible size, relation (7) can further be written

$$\begin{aligned} u(t) &= (1 \otimes \mathbf{w}_u^T)\,(\mathbf{Q}(\omega t)\omega^r\boldsymbol{\nabla}^r \otimes \mathbf{I})\,\mathbf{z} = (\mathbf{Q}(\omega t)\omega^r\boldsymbol{\nabla}^r) \otimes \left(\mathbf{w}_u^T\mathbf{I}\right)\mathbf{z} = \omega^r\,(\mathbf{Q}(\omega t)\boldsymbol{\nabla}^r) \otimes \left(1\mathbf{w}_u^T\right)\mathbf{z} \\ &= \omega^r(\mathbf{Q}(\omega t) \otimes 1)\left(\boldsymbol{\nabla}^r \otimes \mathbf{w}_u^T\right)\mathbf{z} = \omega^r\mathbf{Q}(\omega t)\left(\boldsymbol{\nabla}^r \otimes \mathbf{w}_u^T\right)\mathbf{z}. \end{aligned} \tag{8}$$

The vector of $2N_h + 1$ harmonic coefficients associated with u may also be determined through

$$\mathbf{z}_u = \omega^r\left(\boldsymbol{\nabla}^r \otimes \mathbf{w}_u^T\right)\mathbf{z} = \omega^r\mathbf{B}_u\mathbf{z} \tag{9}$$

and $u(t)$ can equivalently be expressed as a Fourier series from Equations (8) and (9) as

$$u(t) = \mathbf{Q}(\omega t)\mathbf{z}_u = \omega^r\mathbf{Q}(\omega t)\mathbf{B}_u\mathbf{z}. \tag{10}$$

The NFR amplitude a of u is defined for a given value of ω as the maximum absolute value reached by $u(t)$ over a period. Introducing a dimensionless time $\tau = \omega t$ (and replacing the t-dependence of u by an equivalent τ-dependence), the definition

[‡]This choice ensures that the harmonic functions have the same norm, i.e., $2\int_0^{2\pi/\omega}\mathbf{Q}^T(\omega t)\mathbf{Q}(\omega t)dt = \mathbf{I}$.

of a is thus

$$a(\mathbf{z},\omega) = \max_{\tau\in[0,2\pi]} |u(\tau)| = \max_{\tau\in[0,2\pi]} |\omega^r \mathbf{Q}(\tau)\mathbf{B}_u\mathbf{z}|. \tag{11}$$

There are at least two possibilities to compute the amplitude of an NFR. The first one consists in sampling Equation (10) for several values of $\tau \in [0, 2\pi]$ and finding the maximum absolute value among the discrete set of computed values. An alternative consists in solving Equation (11) semi-analytically. This procedure is detailed in the sequel.

Using the properties of the vector of harmonic functions derivatives

$$\mathbf{Q}'(\tau) = \mathbf{Q}(\tau)\boldsymbol{\nabla}, \tag{12}$$

where a prime denotes a derivation with respect to τ, a necessary condition on the dimensionless time at which the maximum of amplitude occurs, $\tau_{\max}(\mathbf{z})$, is given by

$$u'(\tau)\big|_{\tau=\tau_{\max}(\mathbf{z})} = \omega^r \mathbf{Q}(\tau_{\max}(\mathbf{z}))\boldsymbol{\nabla}\mathbf{B}_u\mathbf{z} = 0 \tag{13}$$

and the corresponding amplitude is given by

$$a(\mathbf{z},\omega) = |\omega^r \mathbf{Q}(\tau_{\max}(\mathbf{z}))\mathbf{B}_u\mathbf{z}|. \tag{14}$$

Hence, by solving Equation (13) and inserting its solution into Equation (14), the amplitude can be computed. The procedure to solve Equation (13) is explained in the next section.

2.3 | Companion matrix and extrema of Fourier series

Equation (13) implicitly defines $\tau_{\max}(\mathbf{z})$ (and hence the amplitude of motion). It amounts to finding the roots of a Fourier series. Using the fact that a trigonometric polynomial can be cast to a rational polynomial, Boyd[51] showed that the roots of a Fourier series can be computed from the eigenvalues of a so-called Fourier-Frobenius companion matrix, hereafter simply referred to as "companion matrix" for conciseness.

We now consider that the generalized DoF of interest u has harmonic coefficients

$$\mathbf{z}_u^T = \left[z_0, z_{\mathrm{s},1}, z_{\mathrm{c},1}, \cdots, z_{\mathrm{s},N_h}, z_{\mathrm{c},N_h}\right] \tag{15}$$

so that the derivative of u with respect to the dimensionless time τ is expressed as a Fourier series, and Equation (13) becomes

$$u'(\tau) = \sum_{k=1}^{N_h} \left(-k z_{\mathrm{c},k} \sin(k\tau) + k z_{\mathrm{s},k} \cos(k\tau)\right) = 0 \tag{16}$$

Following Boyd[51], this trigonometric polynomial is converted to a rational polynomial of order $2N_h$ of the complex variable $s = e^{\mathrm{i}\tau}$, where i is the unit imaginary number ($\mathrm{i}^2 = -1$) as

$$u'(\tau) = \frac{1}{e^{\mathrm{i}N_h\tau}} \sum_{k=0}^{2N_h} h_k e^{\mathrm{i}k\tau} = \frac{1}{s^{N_h}} \sum_{k=0}^{2N_h} h_k s^k, \tag{17}$$

where the coefficients h_k are given by

$$h_k = \begin{cases} (N_h - k) z_{\mathrm{s},N_h-k} - \mathrm{i}(N_h - k) z_{\mathrm{c},N_h-k}, & k = 0, \cdots, N_h - 1 \\ 0 & k = N_h \\ (k - N_h) z_{\mathrm{s},k-N_h} + \mathrm{i}(k - N_h) z_{\mathrm{c},k-N_h}, & k = N_h + 1, \cdots, 2N_h \end{cases}. \tag{18}$$

The $2N_h \times 2N_h$ companion matrix $\mathbf{F}$ associated to this polynomial is then given by

$$\mathbf{F} = \begin{bmatrix} 0 & 1 & 0 & \cdots & 0 \\ 0 & 0 & 1 & \cdots & 0 \\ \vdots & \vdots & \vdots & \ddots & \vdots \\ 0 & 0 & 0 & \cdots & 1 \\ -\dfrac{h_0}{h_{2N_h}} & -\dfrac{h_1}{h_{2N_h}} & -\dfrac{h_2}{h_{2N_h}} & \cdots & -\dfrac{h_{2N_h-1}}{h_{2N_h}} \end{bmatrix}. \tag{19}$$

The eigenvalues μ of $\mathbf{F}$ are the roots in s of the ordinary polynomial in the numerator of Equation (17). Those lying on the unit circle are linked to the real roots of the original Fourier series through $\tau_k = \arg(\mu_k)$ where arg is the complex argument

function. This generally yields multiple values of τ_k, since the Fourier series may have multiple extrema. The value of τ that yields the NFR amplitude can eventually simply be determined by computing the response at (real-valued) τ_k for all values of k with Equation (10) and selecting the one(s) with maximum absolute value.

A coefficient h_{2N_h} close or equal to zero can be problematic for the construction of the companion matrix (Equation (19)). This occurs when the coefficients associated with harmonic N_h are small or zero as well in Equation (16). These coefficients can thus be neglected if their absolute value is below a given threshold. An alternative using a generalized eigenvalue problem formulation is also possible[52].

We note that finding the roots of a Fourier series with strictly more than one harmonic corresponds to solving a polynomial equation of order equal to or higher than five. Consequently, owing to the Abel–Ruffini theorem, no closed-form expression of the amplitude as a function of the harmonic coefficients can be obtained for multi-harmonic Fourier series in general. The proposed semi-analytic approach then comes as a practical way to compute this amplitude.

2.3.1 | Discussion

Since two different approaches are available to compute the amplitude of a Fourier series, namely a direct sampling and the companion matrix-based approach, one may wonder which one is the most advantageous.

On the one hand, the nonlinear forces and their associated derivatives are most often computed with an AFT procedure, which requires to compute $\mathbf{x}$ at different time instants. For an accurate computation of the nonlinear forces without aliasing with polynomial nonlinearities, it was shown that the number of sampling points of this AFT, n, should grow linearly with the number of harmonics and the maximum nonlinear exponent, i.e. $n \sim O(N_h)$[53,54]. Hence, since one has to compute $O(N_h)$ dot products of vectors of size $2N_h + 1$ (Equation (10)), the computational complexity of this approach grows as $O(N_h^2)$. It can even be brought down to $O(N_h \log(N_h))$ if a fast Fourier transform is used. A first issue of this approach is that the extrema of the Fourier series may not be located accurately. In addition, the estimated amplitude may feature a nonsmooth character when the sampling point at which the maximum amplitude occurs changes as the system parameters are varied. However, their estimation could be polished using a Newton-Raphson procedure starting from an initial guess[51], thereby resolving these two issues.

On the other hand, the companion matrix-based method requires the computation of the eigenvalues of a matrix of size $2N_h + 1$, therefore the computational complexity grows as $O(N_h^3)$. This approach is thus more expensive in general than a direct sampling. However, it is more accurate and its cost is oftentimes dwarfed by that of the continuation procedure itself, especially if the stability of the response is assessed (for which a much larger eigenvalue problem has to be solved).

Therefore, the two approaches seem viable and rather equivalent for an accurate computation of the NFR amplitude. For problems requiring a very large number of harmonics, the sampling procedure might however be preferable.

3 | TRACKING PROCEDURE

The response of nonlinear structural systems is often assessed with specific features of the NFR, such as the maximum amplitude of the response. Since the latter is influenced by the forcing amplitude, multiple NFRs have to be computed at different forcing levels, making this assessment procedure computationally expensive. A more direct and efficient approach consists in computing only the amplitude extrema of the NFR.

Several procedures were previously proposed in the literature to locate and track amplitude extrema of NFRs. Petrov[36] proposed to incorporate an additional equation to Equation (4) expressing the extremal character of the amplitude with respect to the frequency. This method was nonetheless found to be rather ill-conditioned in some cases[39]. This issue is discussed in Appendix A. Subsequently, Renault et al[38] showed that the extrema of an NFR are characterized by the singularity of the Jacobian of an extended system by drawing a parallel with the characterization of fold bifurcations.

Both approaches in[36,38] approximate the solution of the nonlinear dynamic equilibrium with a multi-harmonic balance method, but compute the harmonic amplitude with a single harmonic. Furthermore, these approaches can only be applied to track the extrema of displacement amplitudes. The aim of this section is to generalize their scope by addressing these two limitations, using the formalism of Renault et al[38]. Furthermore, an efficient procedure based on the AFT[50] is proposed to compute the second derivatives appearing in the problem.

3.1 | Equations for an extremum

To characterize the amplitude extrema of the NFR, an additional mathematical condition for extremality $g_p(\mathbf{z}, \omega) = 0$ is appended to Equation (4), yielding the extended system

$$\mathbf{h}(\mathbf{z}, \omega, \lambda) = \begin{bmatrix} \mathbf{A}(\omega)\mathbf{z} + \mathbf{b}(\mathbf{z}, \omega) - \lambda \mathbf{b}_{\text{ext}} \\ g_p(\mathbf{z}, \omega) \end{bmatrix} = \mathbf{0}. \tag{20}$$

The extremality condition g_p may be the tangent of the NFR[36] or the determinant of the Jacobian of an extended system[38], as shall be shown later. If the external amplitude λ is fixed, Equation (20) defines $N_z + 1$ nonlinear algebraic equations for $N_z + 1$ unknowns and can therefore be solved numerically using (for instance) a Newton-Raphson procedure to find the extrema of the NFR amplitude. By letting λ vary, a one-parameter family of solutions can be computed using, e.g., a continuation procedure. These solutions represent how the extrema of the NFR evolve with the parameter λ.

Including λ as a variable, the Jacobian of the system defined in Equation (20) is

$$\mathbf{J}(\mathbf{z}, \omega) = \left[\frac{\partial \mathbf{h}}{\partial \mathbf{z}}(\mathbf{z}, \omega) \;\; \frac{\partial \mathbf{h}}{\partial \omega}(\mathbf{z}, \omega) \;\; \frac{\partial \mathbf{h}}{\partial \lambda} \right] = \begin{bmatrix} \mathbf{A}(\omega) + \dfrac{\partial \mathbf{b}}{\partial \mathbf{z}}(\mathbf{z}, \omega) & \dfrac{\partial \mathbf{A}(\omega)}{\partial \omega}\mathbf{z} + \dfrac{\partial \mathbf{b}}{\partial \omega}(\mathbf{z}, \omega) & -\mathbf{b}_{\text{ext}} \\ \dfrac{\partial g_p}{\partial \mathbf{z}}(\mathbf{z}, \omega) & \dfrac{\partial g_p}{\partial \omega}(\mathbf{z}, \omega) & 0 \end{bmatrix}, \tag{21}$$

and can be used together with Equation (20) in, e.g., a predictor-corrector continuation scheme[3,4,29,30]. In the remainder of this section, we show how the different parts of the Jacobian can be computed.

3.2 | Derivatives of the matrix of linear forces

The matrix $\mathbf{A}(\omega)$ being given in Equation (5), its first derivative is readily obtained as

$$\frac{\partial \mathbf{A}(\omega)}{\partial \omega} = 2\omega \boldsymbol{\nabla}^2 \otimes \mathbf{M} + \boldsymbol{\nabla} \otimes \mathbf{C}, \tag{22}$$

and its second derivative (which shall be needed later) is

$$\frac{\partial^2 \mathbf{A}(\omega)}{\partial \omega^2} = 2\boldsymbol{\nabla}^2 \otimes \mathbf{M}. \tag{23}$$

3.3 | Alternating Frequency-Time procedure

We now turn to the computation of the nonlinear forces and their derivatives in the frequency domain. The computation of the derivatives of $\mathbf{b}$ is first treated using a classical AFT approach[50]. A dimensionless sampling time vector is formed

$$\boldsymbol{\tau} = \begin{bmatrix} \tau_0 & \tau_1 & \cdots & \tau_{n-1} \end{bmatrix}^T \tag{24}$$

with $\tau_k = 2\pi k/n$. Correspondingly, the matrix of sampled harmonic functions is given by

$$\mathbf{Q}(\boldsymbol{\tau}) = \begin{bmatrix} \mathbf{Q}(\tau_0) \\ \vdots \\ \mathbf{Q}(\tau_{n-1}) \end{bmatrix}. \tag{25}$$

An operator to represent the inverse Fourier transform is used as in[30]

$$\boldsymbol{\Gamma} = \mathbf{Q}(\boldsymbol{\tau}) \otimes \mathbf{I}, \tag{26}$$

and the time-sampled vector of generalized DoFs is computed through

$$\tilde{\mathbf{x}} = \boldsymbol{\Gamma}\mathbf{z} = \left[\mathbf{x}^T(\tau_0), \cdots, \mathbf{x}^T(\tau_{n-1}) \right]^T, \tag{27}$$

where a tilde $(\tilde{\cdot})$ denotes a quantity that is evaluated for each value of the sampling time vector $\boldsymbol{\tau}$.

3.3.1 | Nonlinear forces and their first derivatives in the frequency domain

The vector of nonlinear forces (whose dependence on t is equivalently expressed as a dependence on τ) is readily evaluated in the time domain and can eventually be re-projected in the frequency domain as

$$\mathbf{b} = \boldsymbol{\Gamma}^\dagger \tilde{\mathbf{f}}_{\text{nl}} \left(\tilde{\mathbf{x}}, \dot{\tilde{\mathbf{x}}}, \boldsymbol{\tau} \right) = \boldsymbol{\Gamma}^\dagger \tilde{\mathbf{f}}_{\text{nl}} \left(\boldsymbol{\Gamma}\mathbf{z}, \boldsymbol{\Gamma}(\omega \boldsymbol{\nabla} \otimes \mathbf{I})\mathbf{z}, \boldsymbol{\tau} \right), \tag{28}$$

where the superscript † denotes a pseudoinverse, which in this case is explicitly given by

$$\boldsymbol{\Gamma}^{\dagger} = \frac{2}{n}\boldsymbol{\Gamma}^{T} = \frac{2}{n}\mathbf{Q}^{T}(\boldsymbol{\tau}) \otimes \mathbf{I}. \tag{29}$$

Using the chain rule and Equation (27)[29,30],

$$\frac{\partial \mathbf{b}}{\partial \mathbf{z}} = \boldsymbol{\Gamma}^{\dagger}\left(\frac{\partial \tilde{\mathbf{f}}_{\mathrm{nl}}}{\partial \tilde{\mathbf{x}}}\boldsymbol{\Gamma} + \frac{\partial \tilde{\mathbf{f}}_{\mathrm{nl}}}{\partial \dot{\tilde{\mathbf{x}}}}\boldsymbol{\Gamma}(\omega\boldsymbol{\nabla} \otimes \mathbf{I})\right). \tag{30}$$

The derivative of the nonlinear forces with respect to ω is also given by

$$\frac{\partial \mathbf{b}}{\partial \omega} = \boldsymbol{\Gamma}^{\dagger}\frac{\partial \tilde{\mathbf{f}}_{\mathrm{nl}}}{\partial \dot{\tilde{\mathbf{x}}}}\boldsymbol{\Gamma}(\boldsymbol{\nabla} \otimes \mathbf{I})\mathbf{z}. \tag{31}$$

3.3.2 | Derivatives of matrix-vector products

As anticipated in the introduction and as shall be shown later, second derivatives will be needed to characterize the derivatives of g_p. Before expressing these derivatives, we note that the derivative of a matrix product $\mathbf{Gy}$, for an arbitrary matrix $\mathbf{G}$ and vector $\mathbf{y}$, both functions of $\mathbf{z}$, is given by

$$\frac{\partial}{\partial \mathbf{z}}\left(\mathbf{G}(\mathbf{z})\mathbf{y}(\mathbf{z})\right) = \left\langle \frac{\partial \mathbf{G}}{\partial \mathbf{z}}(\mathbf{z}), \mathbf{y}(\mathbf{z})\right\rangle_{2} + \mathbf{G}(\mathbf{z})\frac{\partial \mathbf{y}}{\partial \mathbf{z}}(\mathbf{z}). \tag{32}$$

$\langle \cdot, \cdot \rangle_n$ denotes here the $n-$mode vector product of a tensor with a vector[55]. Specifically, for the cases treated in this work, the 2-mode vector product of any $N_1 \times N_2 \times N_3$ array $\mathbf{T}$ and vector $\mathbf{u}$ of size N_2 is given by

$$\left(\langle \mathbf{T}, \mathbf{u}\rangle_{2}\right)_{kl} = \sum_{i=1}^{N_2} (\mathbf{T})_{kil}\,(\mathbf{u})_{i}\,, \qquad k = 1, \cdots, N_1, \qquad l = 1, \cdots, N_3, \tag{33}$$

and yields a two-dimensional array. The demonstration of Equation (32) is immediate using the index notation and Equation (33).

The fact that Equation (32) yields a matrix indicates that none of the three-dimensional arrays appearing in this work needs be computed explicitly, but their 2-mode products with vectors do.

3.3.3 | Second derivatives in the frequency domain

To compute the second derivatives of $\mathbf{b}$, the chain rule can be used a second time with Equation (32), yielding

$$\begin{aligned}\frac{\partial^2 \mathbf{b}}{\partial \mathbf{z}\partial \omega} &= \boldsymbol{\Gamma}^{\dagger}\left(\left\langle \frac{\partial^2 \tilde{\mathbf{f}}_{\mathrm{nl}}}{\partial \tilde{\mathbf{x}}\partial \dot{\tilde{\mathbf{x}}}}, \boldsymbol{\Gamma}(\boldsymbol{\nabla} \otimes \mathbf{I})\mathbf{z}\right\rangle_{2}\boldsymbol{\Gamma} + \frac{\partial \tilde{\mathbf{f}}_{\mathrm{nl}}}{\partial \dot{\tilde{\mathbf{x}}}}\boldsymbol{\Gamma}(\boldsymbol{\nabla} \otimes \mathbf{I}) + \left\langle \frac{\partial^2 \tilde{\mathbf{f}}_{\mathrm{nl}}}{\partial \dot{\tilde{\mathbf{x}}}\partial \dot{\tilde{\mathbf{x}}}}, \boldsymbol{\Gamma}(\boldsymbol{\nabla} \otimes \mathbf{I})\mathbf{z}\right\rangle_{2}\boldsymbol{\Gamma}(\omega\boldsymbol{\nabla} \otimes \mathbf{I})\right) \\ &= \boldsymbol{\Gamma}^{\dagger}\left(\frac{1}{\omega}\left\langle \frac{\partial^2 \tilde{\mathbf{f}}_{\mathrm{nl}}}{\partial \tilde{\mathbf{x}}\partial \dot{\tilde{\mathbf{x}}}}, \dot{\tilde{\mathbf{x}}}\right\rangle_{2}\boldsymbol{\Gamma} + \frac{\partial \tilde{\mathbf{f}}_{\mathrm{nl}}}{\partial \dot{\tilde{\mathbf{x}}}}\boldsymbol{\Gamma}(\boldsymbol{\nabla} \otimes \mathbf{I}) + \left\langle \frac{\partial^2 \tilde{\mathbf{f}}_{\mathrm{nl}}}{\partial \dot{\tilde{\mathbf{x}}}\partial \dot{\tilde{\mathbf{x}}}}, \dot{\tilde{\mathbf{x}}}\right\rangle_{2}\boldsymbol{\Gamma}(\boldsymbol{\nabla} \otimes \mathbf{I})\right),\end{aligned} \tag{34}$$

$$\frac{\partial^2 \mathbf{b}}{\partial \omega^2} = \boldsymbol{\Gamma}^{\dagger}\left\langle \frac{\partial^2 \tilde{\mathbf{f}}_{\mathrm{nl}}}{\partial \dot{\tilde{\mathbf{x}}}\partial \dot{\tilde{\mathbf{x}}}}, \boldsymbol{\Gamma}(\boldsymbol{\nabla} \otimes \mathbf{I})\mathbf{z}\right\rangle_{2}\boldsymbol{\Gamma}(\boldsymbol{\nabla} \otimes \mathbf{I})\mathbf{z} = \frac{1}{\omega}\boldsymbol{\Gamma}^{\dagger}\left\langle \frac{\partial^2 \tilde{\mathbf{f}}_{\mathrm{nl}}}{\partial \dot{\tilde{\mathbf{x}}}\partial \dot{\tilde{\mathbf{x}}}}, \dot{\tilde{\mathbf{x}}}\right\rangle_{2}\boldsymbol{\Gamma}(\boldsymbol{\nabla} \otimes \mathbf{I})\mathbf{z} \tag{35}$$

and, considering an arbitrary vector $\mathbf{y}$ of length N_z,

$$\begin{aligned}\left\langle \frac{\partial^2 \mathbf{b}}{\partial \mathbf{z}\partial \mathbf{z}}, \mathbf{y}\right\rangle_{2} &= \boldsymbol{\Gamma}^{\dagger}\left(\left\langle \frac{\partial^2 \tilde{\mathbf{f}}_{\mathrm{nl}}}{\partial \tilde{\mathbf{x}}\partial \tilde{\mathbf{x}}}, \boldsymbol{\Gamma}\mathbf{y}\right\rangle_{2}\boldsymbol{\Gamma} + \left\langle \frac{\partial^2 \tilde{\mathbf{f}}_{\mathrm{nl}}}{\partial \dot{\tilde{\mathbf{x}}}\partial \tilde{\mathbf{x}}}, \boldsymbol{\Gamma}\mathbf{y}\right\rangle_{2}\boldsymbol{\Gamma}(\omega\boldsymbol{\nabla} \otimes \mathbf{I})\right. \\ &\quad \left. + \left\langle \frac{\partial^2 \tilde{\mathbf{f}}_{\mathrm{nl}}}{\partial \tilde{\mathbf{x}}\partial \dot{\tilde{\mathbf{x}}}}, \boldsymbol{\Gamma}(\omega\boldsymbol{\nabla} \otimes \mathbf{I})\mathbf{y}\right\rangle_{2}\boldsymbol{\Gamma} + \left\langle \frac{\partial^2 \tilde{\mathbf{f}}_{\mathrm{nl}}}{\partial \dot{\tilde{\mathbf{x}}}\partial \dot{\tilde{\mathbf{x}}}}, \boldsymbol{\Gamma}(\omega\boldsymbol{\nabla} \otimes \mathbf{I})\mathbf{y}\right\rangle_{2}\boldsymbol{\Gamma}(\omega\boldsymbol{\nabla} \otimes \mathbf{I})\right) \\ &= \boldsymbol{\Gamma}^{\dagger}\left(\left\langle \frac{\partial^2 \tilde{\mathbf{f}}_{\mathrm{nl}}}{\partial \tilde{\mathbf{x}}\partial \tilde{\mathbf{x}}}, \tilde{\mathbf{y}}\right\rangle_{2}\boldsymbol{\Gamma} + \left\langle \frac{\partial^2 \tilde{\mathbf{f}}_{\mathrm{nl}}}{\partial \dot{\tilde{\mathbf{x}}}\partial \tilde{\mathbf{x}}}, \tilde{\mathbf{y}}\right\rangle_{2}\boldsymbol{\Gamma}(\omega\boldsymbol{\nabla} \otimes \mathbf{I})\right. \\ &\quad \left. + \left\langle \frac{\partial^2 \tilde{\mathbf{f}}_{\mathrm{nl}}}{\partial \tilde{\mathbf{x}}\partial \dot{\tilde{\mathbf{x}}}}, \dot{\tilde{\mathbf{y}}}\right\rangle_{2}\boldsymbol{\Gamma} + \left\langle \frac{\partial^2 \tilde{\mathbf{f}}_{\mathrm{nl}}}{\partial \dot{\tilde{\mathbf{x}}}\partial \dot{\tilde{\mathbf{x}}}}, \dot{\tilde{\mathbf{y}}}\right\rangle_{2}\boldsymbol{\Gamma}(\omega\boldsymbol{\nabla} \otimes \mathbf{I})\right),\end{aligned} \tag{36}$$

where $\tilde{\mathbf{y}}$ and $\dot{\tilde{\mathbf{y}}}$ are time-sampled vectors whose Fourier coefficients are $\mathbf{y}$ and $(\omega\boldsymbol{\nabla}\otimes\mathbf{I})\mathbf{y}$, respectively. Each one of these derivatives involves at least one product of a three-dimensional array with a vector. A strategy to compute these products is developed in Section 4.

3.4 | Extremality condition as the singularity of a Jacobian

We now particularize the extremality condition. The formulation of Renault et al[38] is adopted herein, and extended to the case of a frequency-dependent amplitude (which is the case if one is interested in velocity or acceleration extrema). Introducing an amplitude variable $\alpha = a(\mathbf{z}, \omega)$, an extended system is defined from Equation (4) as

$$\tilde{\mathbf{h}}(\mathbf{z}, \omega, \alpha) = \begin{bmatrix} \mathbf{A}(\omega)\mathbf{z} + \mathbf{b}(\mathbf{z}, \omega) - \lambda \mathbf{b}_{\text{ext}} \\ a(\mathbf{z}, \omega) - \alpha \end{bmatrix} = \mathbf{0}. \tag{37}$$

An amplitude extremum of the NFR is defined by the condition

$$\frac{da}{d\omega} = \frac{d\alpha}{d\omega} = 0, \tag{38}$$

with λ fixed. Taking the total derivative of Equation (37) with respect to the frequency and accounting for Equation (38),

$$\frac{d\tilde{\mathbf{h}}}{d\omega} = \frac{\partial \tilde{\mathbf{h}}}{\partial \mathbf{z}} \frac{d\mathbf{z}}{d\omega} + \frac{\partial \tilde{\mathbf{h}}}{\partial \omega} + \frac{\partial \tilde{\mathbf{h}}}{\partial \alpha} \frac{d\alpha}{d\omega} = \tilde{\mathbf{J}} \begin{bmatrix} \frac{d\mathbf{z}}{d\omega} \\ 1 \end{bmatrix} = \mathbf{0}, \tag{39}$$

where the Jacobian $\tilde{\mathbf{J}}$ of the extended system

$$\tilde{\mathbf{J}}(\mathbf{z}, \omega) = \begin{bmatrix} \frac{\partial \tilde{\mathbf{h}}}{\partial \mathbf{z}} & \frac{\partial \tilde{\mathbf{h}}}{\partial \omega} \end{bmatrix} = \begin{bmatrix} \mathbf{A}(\omega) + \frac{\partial \mathbf{b}}{\partial \mathbf{z}}(\mathbf{z}, \omega) & \frac{\partial \mathbf{A}(\omega)}{\partial \omega}\mathbf{z} + \frac{\partial \mathbf{b}}{\partial \omega}(\mathbf{z}, \omega) \\ \frac{\partial a}{\partial \mathbf{z}}(\mathbf{z}, \omega) & \frac{\partial a}{\partial \omega}(\mathbf{z}, \omega) \end{bmatrix} \tag{40}$$

has to be singular at an extremum of a on account of Equation (39). Therefore, the extremality condition $g_p = 0 \Leftrightarrow \det(\tilde{\mathbf{J}}) = 0$, det being the operator giving the determinant of a matrix[38]. It can be remarked that the procedure to compute the first N_z rows of $\tilde{\mathbf{J}}$ has already been outlined for the computation of $\mathbf{J}$.

3.5 | Bordered matrices

We now focus on ways to express the singularity of the Jacobian in Equation (40). Obtaining the determinant of a matrix may be computationally intensive, and its derivatives are not easily expressed. In this work, the function g_p is rather defined implicitly by the solution of a bordered system, similarly to what was used in[29] for bifurcation characterization. One can compute g_p, as well as a pair of related vectors $\mathbf{w}$ and $\mathbf{v}$ by solving the bordered linear systems

$$\begin{bmatrix} \tilde{\mathbf{J}} & \mathbf{p} \\ \mathbf{q}^H & 0 \end{bmatrix} \begin{bmatrix} \mathbf{w} \\ g_p \end{bmatrix} = \begin{bmatrix} \mathbf{0} \\ 1 \end{bmatrix} \tag{41}$$

and

$$\begin{bmatrix} \tilde{\mathbf{J}}^H & \mathbf{q} \\ \mathbf{p}^H & 0 \end{bmatrix} \begin{bmatrix} \mathbf{v} \\ e_p \end{bmatrix} = \begin{bmatrix} \mathbf{0} \\ 1 \end{bmatrix}, \tag{42}$$

where superscript H denotes a Hermitian transpose. When $\tilde{\mathbf{J}}$ is singular and the bordered matrices are not,

$$\det(\tilde{\mathbf{J}}) = 0 \Leftrightarrow g_p = 0 \Leftrightarrow e_p = 0. \tag{43}$$

Furthermore, the bordered matrices are invertible when $\tilde{\mathbf{J}}$ is singular if[46]

$$\mathbf{p} \notin \text{range}(\tilde{\mathbf{J}}), \qquad \mathbf{q} \notin \text{range}(\tilde{\mathbf{J}}^H). \tag{44}$$

These conditions are fairly unrestrictive; $\mathbf{p}$ and $\mathbf{q}$ can thus be chosen arbitrarily or randomly in general. A more systematic selection procedure is detailed hereafter.

3.5.1 | Derivatives of the solution of the bordered system

To compute the Jacobian, Equation (21) requires the derivatives of g_p. Taking the derivative of Equation (41) with respect to an arbitrary parameter ζ, multiplying it by $\mathbf{v}^H$ and accounting for Equation (42),

$$\mathbf{v}^H \frac{\partial \tilde{\mathbf{J}}}{\partial \zeta}\mathbf{w} - e_p \frac{\partial \mathbf{q}^H}{\partial \zeta}\mathbf{w} + \frac{\partial g_p}{\partial \zeta} + g_p \mathbf{v}^H \frac{\partial \mathbf{p}}{\partial \zeta} = 0. \tag{45}$$

Two of these terms vanish if $\mathbf{q}$ and $\mathbf{p}$ do not depend on ζ, or if $e_p = 0$ and $g_p = 0$. If either of these conditions hold, Equation (45) simplifies to

$$\frac{\partial g_p}{\partial \zeta} = -\mathbf{v}^H \frac{\partial \tilde{\mathbf{J}}}{\partial \zeta}\mathbf{w}. \tag{46}$$

Using Equations (21) and (46), the derivative of g_p with respect to ω is given by

$$\frac{\partial g_p}{\partial \omega} = -\mathbf{v}^H \frac{\partial \tilde{\mathbf{J}}}{\partial \omega}\mathbf{w} = -\mathbf{v}^H \begin{bmatrix} \dfrac{\partial \mathbf{A}}{\partial \omega} + \dfrac{\partial^2 \mathbf{b}}{\partial \omega \partial \mathbf{z}} & \dfrac{\partial^2 \mathbf{A}}{\partial \omega^2}\mathbf{z} + \dfrac{\partial^2 \mathbf{b}}{\partial \omega^2} \\ \dfrac{\partial^2 a}{\partial \mathbf{z} \partial \omega} & \dfrac{\partial^2 a}{\partial \omega^2} \end{bmatrix} \mathbf{w}. \tag{47}$$

As for the derivative with respect to $\mathbf{z}$, $\mathbf{w}$ is first partitioned as

$$\mathbf{w}^T = \left[\mathbf{w}_z, w_\omega\right]^T \tag{48}$$

and then Equation (46) becomes, using Equation (32),

$$\frac{\partial g_p}{\partial \mathbf{z}} = -\mathbf{v}^H \left\langle \frac{\partial \tilde{\mathbf{J}}}{\partial \mathbf{z}}, \mathbf{w} \right\rangle_2 = -\mathbf{v}^H \begin{bmatrix} \left\langle \dfrac{\partial^2 \mathbf{b}}{\partial \mathbf{z} \partial \mathbf{z}}, \mathbf{w}_z \right\rangle_2 + \left(\dfrac{\partial \mathbf{A}}{\partial \omega} + \dfrac{\partial^2 \mathbf{b}}{\partial \omega \partial \mathbf{z}} \right) w_\omega \\ \mathbf{w}_z^T \dfrac{\partial^2 a}{\partial \mathbf{z} \partial \mathbf{z}} + w_\omega \dfrac{\partial^2 a}{\partial \omega \partial \mathbf{z}} \end{bmatrix}. \tag{49}$$

The second derivatives of $\mathbf{A}$, $\mathbf{b}$ and a are derived in Sections 3.2, 3.3.3 and 3.6, respectively.

3.5.2 | Adaptation for the bordered matrices

There exists an optimal choice with respect to the condition number consisting in choosing $\mathbf{p}$ and $\mathbf{q}$ as base vectors of the kernels of $\tilde{\mathbf{J}}^H$ and $\tilde{\mathbf{J}}$, respectively[46]. When $g_p \approx 0$ and $e_p \approx 0$, Equations (41) and (42) indicate that $\mathbf{w}$ and $\mathbf{v}$ are close to the kernel of $\tilde{\mathbf{J}}$ and $\tilde{\mathbf{J}}^H$, respectively, making them ideal candidates for an adaptation of the bordered matrices.

The strategy adopted in this work thus consists in keeping $\mathbf{p}$ and $\mathbf{q}$ constant during a correction phase, which allows for using Equation (46). At the end of this phase, g_p and e_p are close to zero, and $\mathbf{p}$ and $\mathbf{q}$ are set equal to $\mathbf{v}$ and $\mathbf{w}$ computed during the last correction step, respectively, for the prediction phase. This makes them close to their optimal counterparts at the next continuation step, thereby guaranteeing a near-optimal condition number and numerical stability. Since g_p and e_p are considered equal to zero to working precision, Equation (46) is also valid for the predictor phase.

At the first continuation step, multiple possibilities can be considered to initialize $\mathbf{p}$ and $\mathbf{q}$. To work with real algebra, they were chosen in this work as the left and right singular vectors, respectively, associated with the smallest singular value of $\tilde{\mathbf{J}}$.

3.6 | Derivatives of the amplitude

To complete the computation of the derivatives of g_p (and thus of the Jacobian), the derivatives of the amplitude remain to be expressed. They can be computed regardless of the method used to determine it (sampling or companion matrix). The method is similar to what was proposed in[56] but is extended to the cases of all parameters of interest here ($\mathbf{z}$ and ω). It is assumed that $\omega > 0$. Differentiating Equation (14) with respect to $\mathbf{z}$ once and twice, using the chain rule and Equation (12), and taking into account the necessary condition on $\tau_{\max}(\mathbf{z})$ given in Equation (13), one gets

$$\frac{\partial a}{\partial \mathbf{z}} = \omega^r \operatorname{sign}(\mathbf{Q}(\tau_{\max}(\mathbf{z}))\mathbf{B}_u\mathbf{z})\mathbf{Q}(\tau_{\max}(\mathbf{z}))\mathbf{B}_u \tag{50}$$

and

$$\frac{\partial^2 a}{\partial \mathbf{z} \partial \mathbf{z}} = \omega^r \operatorname{sign}(\mathbf{Q}(\tau_{\max}(\mathbf{z}))\mathbf{B}_u\mathbf{z}) \Bigg(\mathbf{Q}(\tau_{\max}(\mathbf{z}))\boldsymbol{\nabla}^2\mathbf{B}_u\mathbf{z} \left(\frac{\partial \tau_{\max}}{\partial \mathbf{z}} \right)^T \frac{\partial \tau_{\max}}{\partial \mathbf{z}} + \left(\mathbf{Q}(\tau_{\max}(\mathbf{z}))\boldsymbol{\nabla}\mathbf{B}_u\right)^T \frac{\partial \tau_{\max}}{\partial \mathbf{z}} + \left(\frac{\partial \tau_{\max}}{\partial \mathbf{z}} \right)^T \mathbf{Q}(\tau_{\max}(\mathbf{z}))\boldsymbol{\nabla}\mathbf{B}_u \Bigg), \tag{51}$$

respectively. The latter equality assumes $a \neq 0$ in order to neglect the effect of the sign function and its differentiation issues at zero, which holds true for most cases of interest. A notable exception concerns the antiresonances of conservative systems, for

which the amplitude extremality condition can simply be replaced by the condition $a = 0$[38]. The derivatives with respect to ω are obtained from Equations (14) and (50) as

$$\frac{\partial a}{\partial \omega} = r\omega^{r-1} \left| \mathbf{Q}(\tau_{\max}(\mathbf{z}))\mathbf{B}_u \mathbf{z} \right|, \tag{52}$$

$$\frac{\partial^2 a}{\partial \omega^2} = r(r-1)\omega^{r-2} \left| \mathbf{Q}(\tau_{\max}(\mathbf{z}))\mathbf{B}_u \mathbf{z} \right| \tag{53}$$

and

$$\frac{\partial^2 a}{\partial \omega \partial \mathbf{z}} = r\omega^{r-1} \operatorname{sign}(\mathbf{Q}(\tau_{\max}(\mathbf{z}))\mathbf{B}_u \mathbf{z}) \mathbf{Q}(\tau_{\max}(\mathbf{z}))\mathbf{B}_u. \tag{54}$$

The last quantity to determine is the derivative of $\tau_{\max}$ with respect to $\mathbf{z}$. Writing out Equation (13) with an explicit dependence of $\tau_{\max}$ on $\mathbf{z}_u$ reads

$$\mathbf{Q}\left(\tau_{\max}(\mathbf{z}_u)\right) \boldsymbol{\nabla} \mathbf{z}_u = 0 \tag{55}$$

Taking the total derivative with respect to $\mathbf{z}_u$ of this condition yields

$$\mathbf{Q}\left(\tau_{\max}(\mathbf{z}_u)\right) \boldsymbol{\nabla}^2 \mathbf{z}_u \frac{\partial \tau_{\max}}{\partial \mathbf{z}_u} + \mathbf{Q}\left(\tau_{\max}(\mathbf{z}_u)\right) \boldsymbol{\nabla} = 0. \tag{56}$$

Hence

$$\frac{\partial \tau_{\max}}{\partial \mathbf{z}_u} = -\frac{\mathbf{Q}\left(\tau_{\max}(\mathbf{z}_u)\right) \boldsymbol{\nabla}}{\mathbf{Q}\left(\tau_{\max}(\mathbf{z}_u)\right) \boldsymbol{\nabla}^2 \mathbf{z}_u}. \tag{57}$$

Since $\mathbf{Q}\left(\tau_{\max}(\mathbf{z}_u)\right) \boldsymbol{\nabla}^2 \mathbf{z}_u = u''(\tau_{\max})$ and since we are interested in extrema of the Fourier series, this quantity is nonzero (except in trivial or degenerate cases). Eventually, the derivative of $\tau_{\max}$ with respect to $\mathbf{z}$ may be expressed as

$$\frac{\partial \tau_{\max}}{\partial \mathbf{z}} = \frac{\partial \tau_{\max}}{\partial \mathbf{z}_u} \frac{\partial \mathbf{z}_u}{\partial \mathbf{z}} = \omega^r \frac{\partial \tau_{\max}}{\partial \mathbf{z}_u} \mathbf{B}_u. \tag{58}$$

There may be multiple values $\tau_{\max}$ which satisfy Equation (13) while also corresponding to a maximum of amplitude. The derivatives evaluated at these dimensionless times may differ and thus multiple derivatives values seem possible. This translates the fact that the amplitude is not differentiable in such situations[57]. For a Fourier series with both even and odd harmonics, this situation is nongeneric (i.e., there is generically only one amplitude maximum). However, this always occurs when the Fourier series exclusively contains even or odd harmonics. The latter case is of relevance since it corresponds to symmetric responses of systems with symmetric nonlinearities. Nevertheless, this differentiability issue only concerns the derivatives of harmonic coefficient of different parity from the Fourier series, as is shown in B. Since for symmetric responses only the odd Fourier coefficients are needed while the even ones are (theoretically) equal to zero, the problematic derivatives with respect to the latter can be ignored. Thus, if multiple amplitude maxima occur, the practical approach used in this work is to select one of them arbitrarily and use it to compute the derivatives.

4 | NONLINEAR FORCES AND THEIR DERIVATIVES IN THE TIME DOMAIN

A procedure to compute the time-domain expression of the nonlinear forces and their derivatives is now outlined. In particular, an efficient way to compute the 2-mode products is proposed. To make the expression of the derivatives as explicit as possible, a generic form for a nonlinearity having no internal states is now introduced. It is given by

$$\mathbf{f}_p(\mathbf{x}(\tau), \dot{\mathbf{x}}(\tau), \tau) = \mathbf{b}_p f_p\left(\mathbf{C}_p \mathbf{x}(\tau), \mathbf{D}_p \dot{\mathbf{x}}(\tau), \tau\right) = \mathbf{b}_p f_p\left(\xi_1(\tau), \cdots, \xi_m(\tau), \eta_1(\tau), \cdots \eta_l(\tau), \tau\right), \tag{59}$$

where $\mathbf{b}_p$ is an $N_x \times 1$ vector that describes the spatial distribution of the nonlinear force on the structure, $\mathbf{C}_p$ is an $m \times N_x$ matrix that gives the local strain-like quantities $\xi_1, \cdots, \xi_m$ in the nonlinear element, such that

$$\mathbf{C}_p \mathbf{x} = \left[\xi_1, \cdots, \xi_m\right]^T = \boldsymbol{\xi} \tag{60}$$

and $\mathbf{D}_p$ is an $l \times N_x$ matrix that gives the local strain rate-like quantities $\eta_1, \cdots, \eta_l$ in the nonlinear element, such that

$$\mathbf{D}_p \dot{\mathbf{x}} = \left[\eta_1, \cdots, \eta_l\right]^T = \boldsymbol{\eta}. \tag{61}$$

The two latter matrices are used to compute the arguments of the nonlinear functional form f_p given in Equation (59), which can be an arbitrary function. Summing up multiple nonlinearities of this form allows for the representation of arbitrary structural

nonlinearities. In particular, if there are N_x such nonlinearities, and if for $p = 1, \cdots, N_x$, $\mathbf{b}_p = \mathbf{e}_p$ (the p^{th} canonical basis vector of $\mathbb{R}^{N_x}$), $\mathbf{C}_p = \mathbf{I}$ and $\mathbf{D}_p = \mathbf{I}$, the most general representation of a nonlinear vector function is retrieved:

$$\mathbf{f}_{\text{nl}}(\mathbf{x}, \dot{\mathbf{x}}, \tau) = \sum_{p=1}^{N_x} \mathbf{b}_p f_p(\mathbf{C}_p\mathbf{x}, \mathbf{D}_p\dot{\mathbf{x}}, \tau) = \sum_{p=1}^{N_x} \mathbf{e}_p f_p(\mathbf{x}, \dot{\mathbf{x}}, \tau) = \begin{bmatrix} f_1(x_1, \cdots, x_{N_x}, \dot{x}_1, \cdots, \dot{x}_{N_x}, \tau) \\ \vdots \\ f_{N_x}(x_1, \cdots, x_{N_x}, \dot{x}_1, \cdots, \dot{x}_{N_x}, \tau) \end{bmatrix}. \tag{62}$$

This formulation is particularly attractive for localized nonlinearities, for which typically $\mathbf{b}_p = \mathbf{C}_p$ and/or $\mathbf{b}_p = \mathbf{D}_p$ is a Boolean vector indicating the location of the nonlinear element[4].

The focus is put on a single nonlinearity in the sequel, but the generalization to multiple nonlinearities is immediate by summation. The nonlinear function can be evaluated at each of the n time instants, yielding a vector $\tilde{f}_p = f_p(\boldsymbol{\tau})$ of length n, which can be related to the sampled nonlinear structural forces by

$$\tilde{\mathbf{f}}_p = \tilde{f}_p \otimes \mathbf{b}_p. \tag{63}$$

The derivatives of f_p with respect to $\boldsymbol{\xi}$ are evaluated for each time instant and gathered in a block diagonal $n \times nm$ matrix $\partial \tilde{f}_p / \partial \tilde{\boldsymbol{\xi}}$, which is linked to the derivatives of $\tilde{\mathbf{f}}_p$ with respect to $\tilde{\mathbf{x}}$ by

$$\frac{\partial \tilde{\mathbf{f}}_p}{\partial \tilde{\mathbf{x}}} = \left(\frac{\partial \tilde{f}_p}{\partial \tilde{\boldsymbol{\xi}}} \frac{\partial \tilde{\boldsymbol{\xi}}}{\partial \tilde{\mathbf{x}}} \right) \otimes \mathbf{b}_p = \left(\frac{\partial \tilde{f}_p}{\partial \tilde{\boldsymbol{\xi}}} (\mathbf{I} \otimes \mathbf{C}_p) \right) \otimes \mathbf{b}_p. \tag{64}$$

Similarly, for the derivatives of $\tilde{\mathbf{f}}_p$ with respect to $\tilde{\dot{\mathbf{x}}}$,

$$\frac{\partial \tilde{\mathbf{f}}_p}{\partial \tilde{\dot{\mathbf{x}}}} = \left(\frac{\partial \tilde{f}_p}{\partial \tilde{\boldsymbol{\eta}}} \frac{\partial \tilde{\boldsymbol{\eta}}}{\partial \tilde{\dot{\mathbf{x}}}} \right) \otimes \mathbf{b}_p = \left(\frac{\partial \tilde{f}_p}{\partial \tilde{\boldsymbol{\eta}}} (\mathbf{I} \otimes \mathbf{D}_p) \right) \otimes \mathbf{b}_p. \tag{65}$$

Finally, to compute the second derivatives, the Hessian matrix of f_p is first partitioned as

$$\frac{\partial^2 f_p}{\partial(\boldsymbol{\xi}, \boldsymbol{\eta}) \partial(\boldsymbol{\xi}, \boldsymbol{\eta})} = \begin{bmatrix} \dfrac{\partial^2 f_p}{\partial \boldsymbol{\xi} \partial \boldsymbol{\xi}} & \dfrac{\partial^2 f_p}{\partial \boldsymbol{\xi} \partial \boldsymbol{\eta}} \\ \dfrac{\partial^2 f_p}{\partial \boldsymbol{\eta} \partial \boldsymbol{\xi}} & \dfrac{\partial^2 f_p}{\partial \boldsymbol{\eta} \partial \boldsymbol{\eta}} \end{bmatrix}, \tag{66}$$

and the following row vector quantities are introduced

$$\mathbf{H}_{\mathbf{xx};\mathbf{y}}(\tau) = \left(\frac{\partial^2 f_p}{\partial \boldsymbol{\xi} \partial \boldsymbol{\xi}} \mathbf{C}_p \mathbf{y}(\tau) \right)^T, \tag{67}$$

$$\mathbf{H}_{\mathbf{x\dot{x}};\mathbf{y}}(\tau) = \left(\frac{\partial^2 f_p}{\partial \boldsymbol{\xi} \partial \boldsymbol{\eta}} \mathbf{D}_p \mathbf{y}(\tau) \right)^T, \tag{68}$$

$$\mathbf{H}_{\mathbf{\dot{x}x};\mathbf{y}}(\tau) = \left(\frac{\partial^2 f_p}{\partial \boldsymbol{\eta} \partial \boldsymbol{\xi}} \mathbf{C}_p \mathbf{y}(\tau) \right)^T, \tag{69}$$

and

$$\mathbf{H}_{\mathbf{\dot{x}\dot{x}};\mathbf{y}}(\tau) = \left(\frac{\partial^2 f_p}{\partial \boldsymbol{\eta} \partial \boldsymbol{\eta}} \mathbf{D}_p \mathbf{y}(\tau) \right)^T. \tag{70}$$

These vectors can then be evaluated for each time instant and gathered in $n \times mn$ and $n \times ln$ block diagonal matrices (similarly to the first derivatives), denoted with a tilde over the corresponding quantities given in Equations (67)-(70). The required 2-mode products are finally obtained as

$$\left\langle \frac{\partial^2 \tilde{\mathbf{f}}_{\text{nl}}}{\partial \tilde{\mathbf{x}} \partial \tilde{\mathbf{x}}}, \tilde{\mathbf{y}} \right\rangle_2 = \left(\tilde{\mathbf{H}}_{\mathbf{xx};\mathbf{y}} (\mathbf{I} \otimes \mathbf{C}_p) \right) \otimes \mathbf{b}_p, \tag{71}$$

$$\left\langle \frac{\partial^2 \tilde{\mathbf{f}}_{\text{nl}}}{\partial \tilde{\mathbf{x}} \partial \tilde{\dot{\mathbf{x}}}}, \tilde{\mathbf{y}} \right\rangle_2 = \left(\tilde{\mathbf{H}}_{\mathbf{x\dot{x}};\mathbf{y}} (\mathbf{I} \otimes \mathbf{C}_p) \right) \otimes \mathbf{b}_p, \tag{72}$$

$$\left\langle \frac{\partial^2 \tilde{\mathbf{f}}_{\text{nl}}}{\partial \tilde{\dot{\mathbf{x}}} \partial \tilde{\mathbf{x}}}, \tilde{\mathbf{y}} \right\rangle_2 = \left(\tilde{\mathbf{H}}_{\mathbf{\dot{x}x};\mathbf{y}} (\mathbf{I} \otimes \mathbf{D}_p) \right) \otimes \mathbf{b}_p, \tag{73}$$

and

$$\left\langle \frac{\partial^2 \tilde{\mathbf{f}}_{\text{nl}}}{\partial \tilde{\dot{\mathbf{x}}} \partial \tilde{\dot{\mathbf{x}}}}, \tilde{\mathbf{y}} \right\rangle_2 = \left(\tilde{\mathbf{H}}_{\dot{\mathbf{x}}\dot{\mathbf{x}};\mathbf{y}} (\mathbf{I} \otimes \mathbf{D}_p) \right) \otimes \mathbf{b}_p. \tag{74}$$

5 | ADDITIONAL NUMERICAL FEATURES

Before illustrating the proposed method with several examples, a few features of the continuation scheme are discussed.

5.1 | Stability and bifurcation analysis

The local stability of the solutions obtained by continuation can be assessed as well. Since only the harmonic coefficients $\mathbf{z}$ are associated with dynamic governing equations in Equation (4), the stability analysis is identical to the classical one associated with NFR computations. Hill's method can thus be used[4,29]. As for bifurcation analysis, the same remarks hold if ω is considered as the bifurcation parameter. It should nonetheless be noted that fold bifurcations are not associated with a vertical tangency of the locus of extrema with respect to the frequency axis; the component of the tangent vector associated with the frequency can thus no longer be used as a test function to detect fold bifurcations.

5.2 | Computational complexity

Compared to the case of an NFR, we note that the computation of the system characterizing an extremum (Equation (20)) and its Jacobian (Equation (21)) require the following additional significant operations:

1. the solution of two linear systems (Equations (41) and (42)), although the factorization of only one matrix is required, and
2. the computation of up to six 2-mode vector products (Equations (34)-(36)) during the AFT procedure.

The relative cost of these operations highly depends on the nature of the nonlinearities (in particular, whether they are distributed or localized, and whether they depend simultaneously on $\mathbf{x}$ and $\dot{\mathbf{x}}$), but this cost will always be superior to that of an NFR evaluation by a near-constant factor (this constant depending on the problem at hand).

6 | EXAMPLES

The method is illustrated with three examples: a Helmholtz-Duffing oscillator, a two-DoF structure, and a doubly clamped beam. In the first two examples, arbitrary units are used. In all examples, $N_h = 9$ harmonics are used with a number of AFT points $n = 64$ sufficient to avoid aliasing[53,54]. This choice was made after a convergence study, showing in all examples a negligible relative difference in all quantities (less than 10^{-6}) between further increments of the number of harmonics. The adaptive scheme for the continuation step length proposed in[58] was used with an ideal number of correction iterations $K_{\text{opt}} = 3$, an ideal hyperangle between tangent and secant predictors θ_{opt} satisfying $1 + \cos(\theta_{\text{opt}}) = 1.999$, and respective geometric weighting parameters for the adaptation law $\beta_1 = 0.2$ and $\beta_2 = 0.8$.

Some results obtained by the extremum tracking approach are compared to phase resonance, in a similar spirit to[39]. However, a conventional definition of phase resonance as phase quadrature is used herein. The proposed procedure is also compared to its single-harmonic counterpart[38], which can be obtained from the framework of this paper by selecting specific lines of the matrix $\mathbf{B}_u$ (Equation (9)).

6.1 | Helmholtz-Duffing oscillator

A Helmholtz-Duffing oscillator is taken as a first example to illustrate the results. The equation of motion reads

$$m\ddot{x} + c\dot{x} + kx + k_2 x^2 + k_3 x^3 = \lambda \sin(\omega t), \tag{75}$$

with $m = 1$, $c = 0.1$, $k = 1$, $k_2 = 1.6$, and $k_3 = 1$. The response of the system is analyzed for five different forcing amplitudes λ linearly increasing up to 0.15. Figure 1 displays the NFRs of the system under different forcing amplitudes, as well as the

results of the proposed tracking procedure applied to the primary resonance amplitude. In Figure 1a, one observes that the locus of resonant peaks corresponds indeed to the place where the NFR amplitude has a horizontal tangent, and that the softening-hardening character of the oscillator is well captured. In Figure 1b, one can clearly see that this locus traces the maximum of the NFR amplitude, as expected.

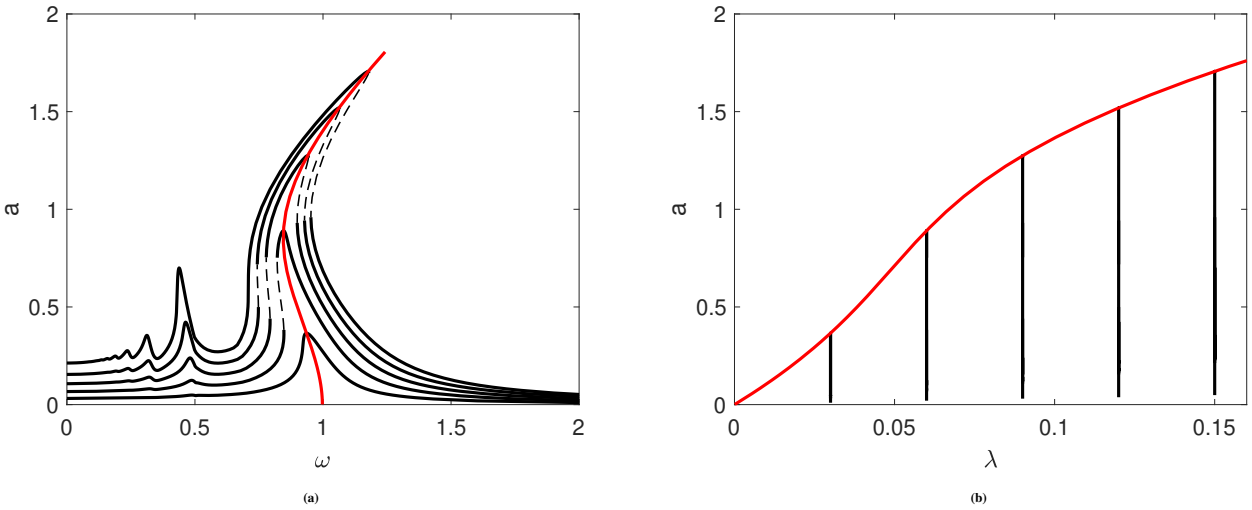

Figure 1 Set of NFRs of the Helmholtz-Duffing oscillator (—) and locus of resonant peaks (—): projection on the (ω, a) plane (a) and projection on the (λ, a) plane (b). —: stable solution, - - -: unstable solution.

The single-harmonic approach[36,38] and phase resonance approach[39] yield sensibly similar results to the proposed approach in this case. They are not displayed in Figure 1 because the curves are indistinguishable at this scale. The agreement between the different methods can be understood by looking at the NFR features for an external forcing amplitude of 0.15 in Figure 2. Figure 2a compares the multi-harmonic amplitude (Equation (11)) to the harmonic amplitudes defined by

$$a_0 = |z_0|, \qquad a_n = \sqrt{z_{\mathrm{s},n}^2 + z_{\mathrm{c},n}^2}, \; n \geq 1, \tag{76}$$

and shows that the participation of harmonics to the response is non-negligible. However, the multi-harmonic amplitude maximum occurs for a frequency which is very close to that of the maximum amplitude of the first harmonic, explaining why the single-harmonic approach performs well in spite of the multi-harmonic nature of the motion. Figure 2b highlights the closeness of the amplitude resonance frequency with that of the phase resonance frequency where the phase of the first harmonic, given by

$$\theta = \arctan\left(\frac{-z_{\mathrm{c},1}}{z_{\mathrm{s},1}}\right), \tag{77}$$

reaches $\pi/2$.

6.2 | Two-degree-of-freedom system

A second example is a two-DoF system governed by the following equations:

$$\begin{cases} m_1\ddot{x}_1 + c_1\dot{x}_1 + c_{12}(\dot{x}_1 - \dot{x}_2) + k_1x_1 + k_{12}(x_1 - x_2) + k_3x_1^3 = \lambda\sin(\omega t) \\ m_2\ddot{x}_2 + c_2\dot{x}_2 + c_{12}(\dot{x}_2 - \dot{x}_1) + k_2x_2 + k_{12}(x_2 - x_1) = 0 \end{cases}, \tag{78}$$

with $m_1 = m_2 = 1$, $k_1 = k_2 = 1$, $k_{21} = 7$ and $k_3 = 0.5$. The viscous damping coefficients c_1, c_2 and c_{12} are adapted to prescribe a desired modal damping on the two modes of the underlying linear system.

The conservative system is first studied by setting $c_1 = c_2 = c_{12} = 0$ and $\lambda = 0$. We note that the two (undamped) natural frequencies of the underlying linear system are $\omega_1 = 1$ and $\omega_2 = 3.87$. Figure 3a presents the frequency-energy plot obtained

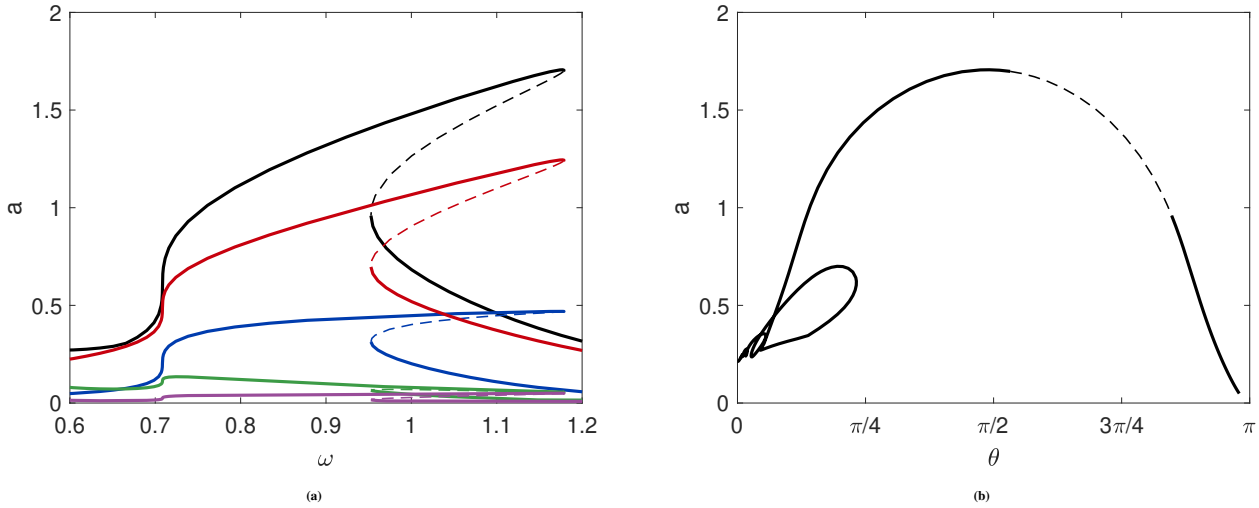

Figure 2 NFR of the Helmholtz-Duffing oscillator at $\lambda = 0.15$: multi-harmonic amplitude (—), amplitude of the zeroth (—), first (—), second (—) and third (—) harmonics (a), and phase of the first harmonic against multi-harmonic amplitude (b). —: stable solution, - - -: unstable solution.

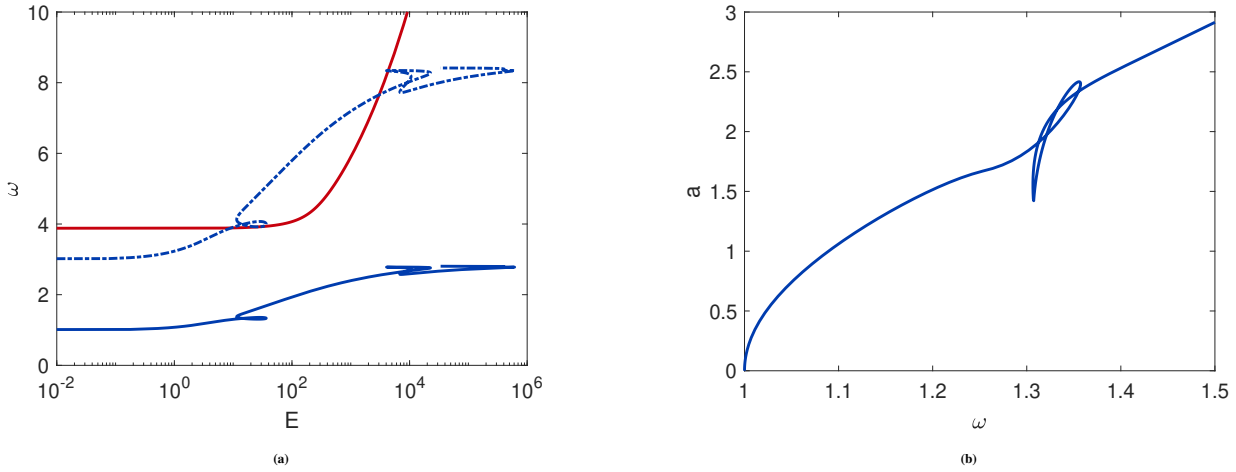

Figure 3 Frequency-energy plot (a) and backbone curve for the first DoF (b) of the conservative two-DoF system: first mode (—: frequency multiplied by one, - - -: frequency multiplied by three), second mode (—).

by computing the nonlinear normal modes of the system with the HB-based method described in[59]. The energy is computed as

$$E = \frac{1}{2}m_1\dot{x}_1^2(0) + \frac{1}{2}m_2\dot{x}_2^2(0) + \frac{1}{2}k_1x_1^2(0) + \frac{1}{2}k_2x_2^2(0) + \frac{1}{2}k_{12}(x_1(0) - x_2(0))^2 + \frac{1}{4}k_3x_1^4(0). \tag{79}$$

The frequency-energy plot clearly highlights the occurrence of modal interactions. The 3:1 modal interaction occurring around $E = 10$ and signaled by the α-shaped loop of the first mode is of particular interest here. Figure 3b indicates that such a modal interaction can be expected when the frequency of excitation reaches $\omega \approx 1.35$ and the amplitude of x_1 reaches $a \approx 2.4$ in the forced, damped system, as long as the damping is kept low enough to make the results of this analysis relevant.

Moving on to the forced, damped system, a first lightly-damped case is studied, where the modal damping on both modes is set to 0.5%. The amplitude of the first DoF is considered under forcing amplitudes going up to $\lambda = 1$. Figure 4 depicts the NFRs of the system, as well as the results of multiple tracking procedures applied to both modes, namely, single-harmonic and multi-harmonic amplitude extrema tracking, and phase resonance tracking. Stability information and bifurcations are not always

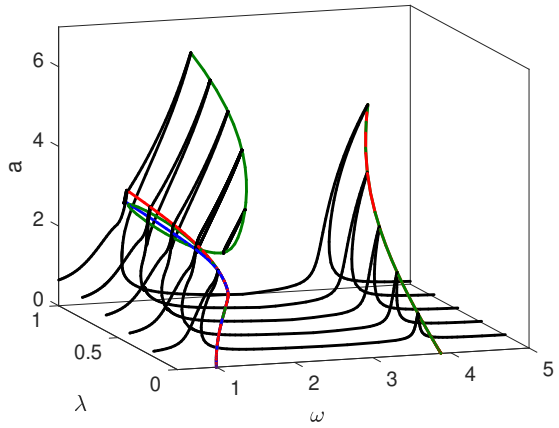

Figure 4 Set of NFRs of the first DoF of the two-DoF system with 0.5% modal damping (—), single-amplitude extrema (—), multi-amplitude extrema (—) and phase resonance (—).

displayed throughout the discussion of this example given the complexity of the curves. All methods agree almost perfectly for the second mode. However, the amplitude extrema tracking procedures do not appear to follow the primary resonance of the first mode in this case, whereas the phase resonance tracking procedure does.

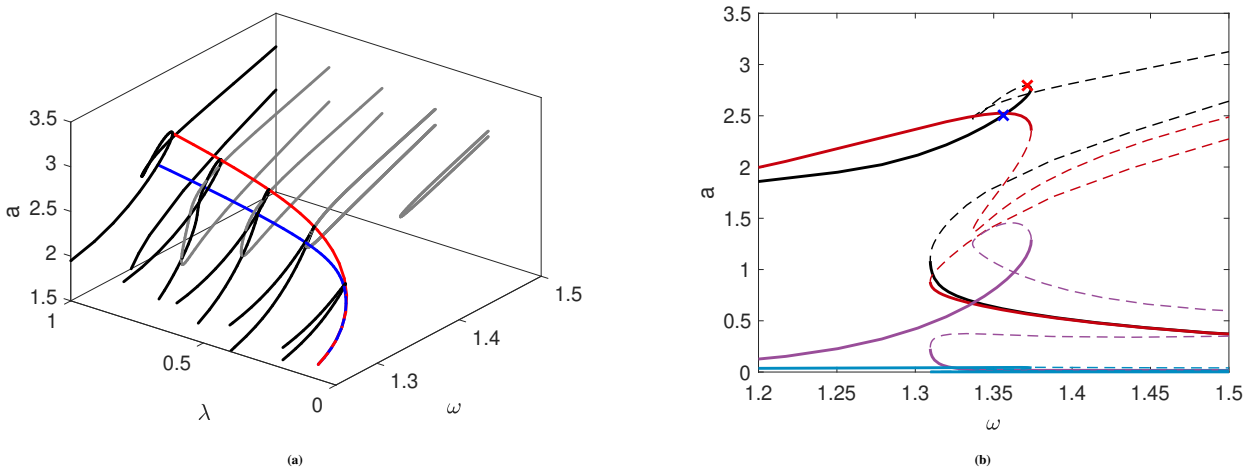

Figure 5 Set of NFRs of the first DoF of the two-DoF system with 0.5% modal damping (—: main branch, —: isola), single-harmonic amplitude extrema (—) and multi-harmonic amplitude extrema (—), close-up on the modal interaction (a) and NFR at $\lambda = 1$: multi-harmonic amplitude (—), amplitude of the first (—), third (—) and fifth (—) harmonics (b). —: stable solution, - - -: unstable solution.

A close-up on the NFRs around the extrema tracking curves is shown in Figure 5a. The multi-harmonic version proposed herein tracks a local maximum that occurs on a small loop, whereas the single-harmonic tracking procedure does not appear to localize any amplitude extremum accurately. This situation can be better understood by looking at the harmonics for, e.g., $\lambda = 1$ in Figure 5b. One can see that the amplitude of the first harmonic drops in favor of the third one, which is a signature of a 3:1 superharmonic resonance, in this case of the second mode. This drop causes the single-harmonic tracking procedure to be stuck before the superharmonic resonance, at the local maximum of the first harmonic amplitude. The multi-harmonic tracking stays on the amplitude peak associated with the superharmonic resonance. The two procedures switch from the primary resonance of the first mode to the superharmonic resonance of the second mode when these two resonances meet, i.e., at the

internal resonance. This example serves as a reminder that the proposed procedures are merely able to track local extrema of the amplitude. Of course, when restarted on the main peak beyond the internal resonance, these two procedures are also able to track the amplitude maxima of the first mode.

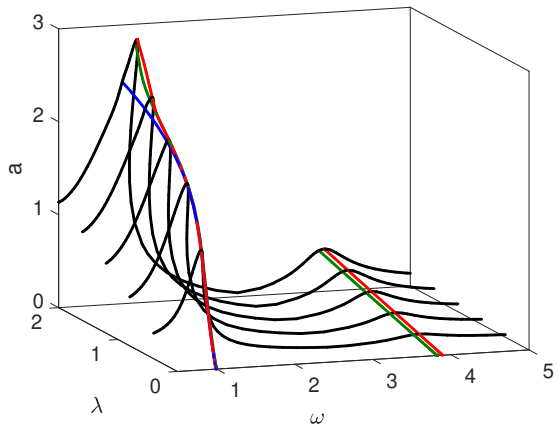

Figure 6 Set of NFRs of the first DoF of the two-DoF system with 7.5% modal damping (—), single-harmonic amplitude extrema (—), multi-harmonic amplitude extrema (—) and phase resonance (—).

The effect of the internal resonance can be mitigated when the structural damping is increased. Figure 6 presents the results of the tracking procedures when the modal damping on both modes is increased to 7.5%. In this case, while single-harmonic tracking is not able to overcome the internal resonance, the proposed multi-harmonic version does, and accurately tracks the maxima associated with the first mode beyond the internal resonance. It can also be observed that the phase resonance becomes less accurate to characterize the amplitude resonance, given the moderate amount of damping in the structure.

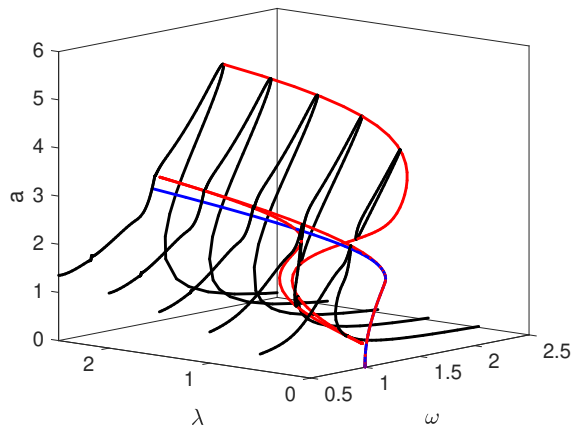

Figure 7 Set of NFRs of the first DoF of the two-DoF system with 0.5% modal damping and a nonlinear cubic damping element (—), single-harmonic amplitude extrema (—) and multi-harmonic amplitude extrema (—).

The influence of the superharmonic resonance can also be mitigated in the presence of nonlinear damping. When a cubic damping element is added between the two DoFs, i.e., when Equation (78) is replaced by

$$\begin{cases} m_1\ddot{x}_1 + c_1\dot{x}_1 + c_{12}(\dot{x}_1 - \dot{x}_2) + c_3(\dot{x}_1 - \dot{x}_2)^3 + k_1x_1 + k_{12}(x_1 - x_2) + k_3x_1^3 = \lambda\sin(\omega t) \\ m_2\ddot{x}_2 + c_2\dot{x}_2 + c_{12}(\dot{x}_2 - \dot{x}_1) + c_3(\dot{x}_2 - \dot{x}_1)^3 + k_2x_2 + k_{12}(x_2 - x_1) = 0 \end{cases}, \tag{80}$$

with $c_3 = 0.0025$, Figure 7 shows that the proposed multi-harmonic tracking procedure is once again able to track the amplitude maxima associated with the first mode, whereas the single-harmonic one stays locked onto the superharmonic resonance. The shape of this curve is relatively complex due to the dynamics exhibited by the structure at the modal interaction. It can show up to seven simultaneous extrema for a given forcing level. An example is given in Figure 8a with the NFR of the system at $\lambda = 1.05$. In addition, the method also reveals the presence of a peculiar isola due to the 3:1 superharmonic resonance of the second mode, inside the main resonance peak of the first mode, that can be observed in Figure 8b when the system is forced with $\lambda = 1.1$. We note that this internal isola also exists without nonlinear damping, but is then not captured by the proposed tracking method.

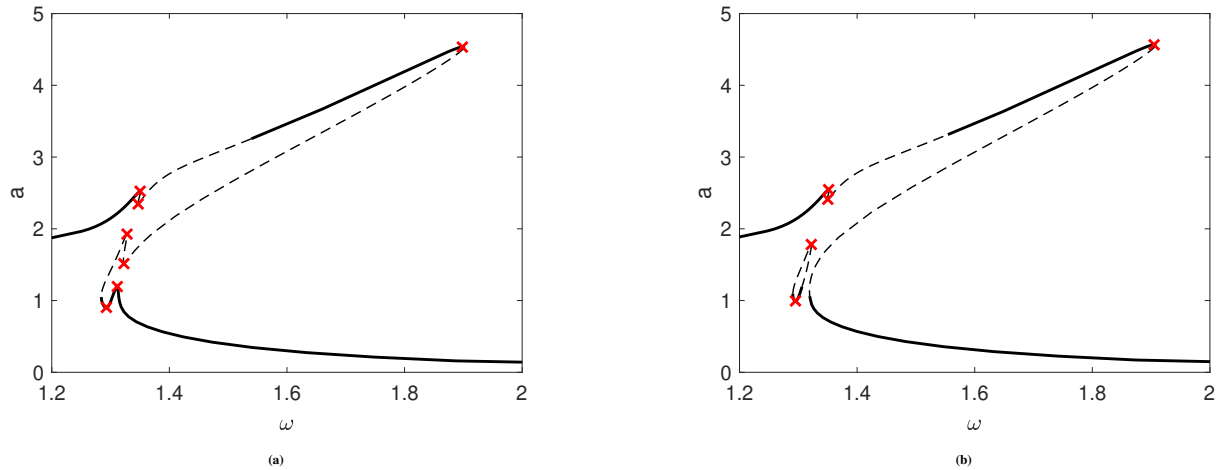

Figure 8 NFRs of the first DoF of the two-DoF system with 0.5% modal damping and a nonlinear cubic damping element (—) at $\lambda = 1.05$ (a) and $\lambda = 1.1$ (b) and extrema found by the tracking procedure (×). —: stable solution, - - -: unstable solution.

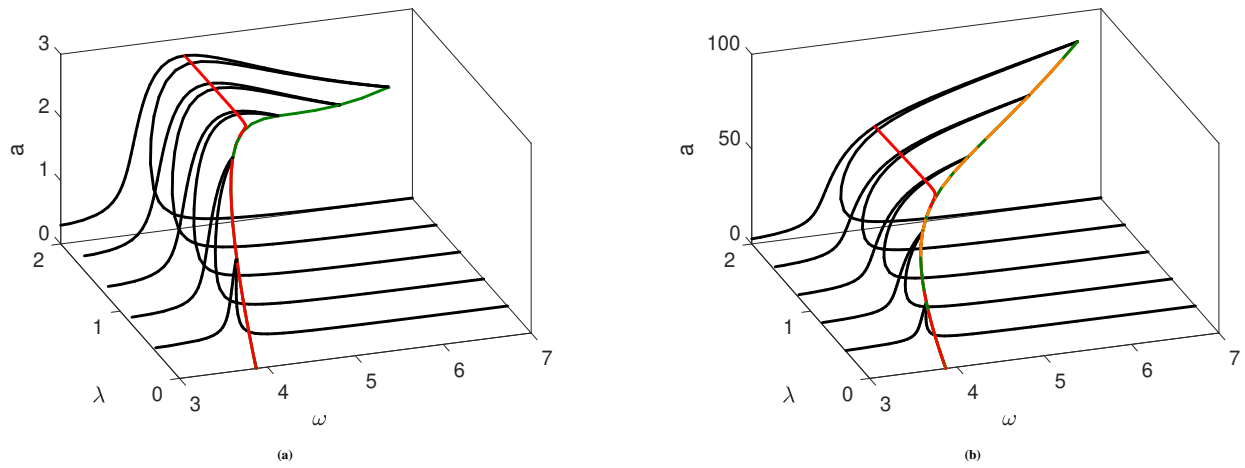

Figure 9 Set of NFRs of the displacement (a) and acceleration (b) associated with the second DoF of the two-DoF system with 0.5% modal damping (—), multi-harmonic displacement extrema (—), multi-harmonic acceleration extrema (—) and phase resonance (—).

The local nature of the proposed method is not always an issue depending on the objective at hand. For instance, when the amplitude extrema of the second DoF are followed starting from the second mode, the proposed method yields the results

displayed in Figure 9a. The NFR shows a peculiar shape, where the peak of the second mode bends and eventually folds and decreases in amplitude. This behavior is due to the localization of the second mode on the first DoF as the forcing amplitude increases. This creates an amplitude maximum, whose amplitude is higher than the tip of the peak indicated by the phase resonance. The tracking procedure is able to accurately follow this maximum which, if one is interested in the worst-case amplitude around the second mode resonance, is a relevant feature to track.

The folded peak does not appear in the acceleration of the second DoF. Figure 9b then shows that the proposed tracking method (with $r = 2$ in Equation (8)) is able to follow the locus of acceleration peaks, which is much closer to phase resonance. This example also shows that displacement and acceleration amplitude extrema may not be close in all cases.

6.3 | Doubly clamped beam

The last example is a doubly clamped steel beam with a rectangular cross section excited at one fifth of its span and featuring a distributed geometrical nonlinearity. The dynamics of the bare beam are first analyzed, and a nonlinear tuned vibration absorber (NLTVA)[10] is then added to the system in an attempt to reduce the vibrations of the system.

6.3.1 | Model

The beam is modeled using Euler-Bernoulli kinematics. In the considered examples, the beam features transversal displacements of the order of its thickness; a von Kàrmàn formulation was thus adopted to express the nonlinear strain. Figure 10a depicts the beam, and its geometrical and material characteristics are gathered in Table 1.

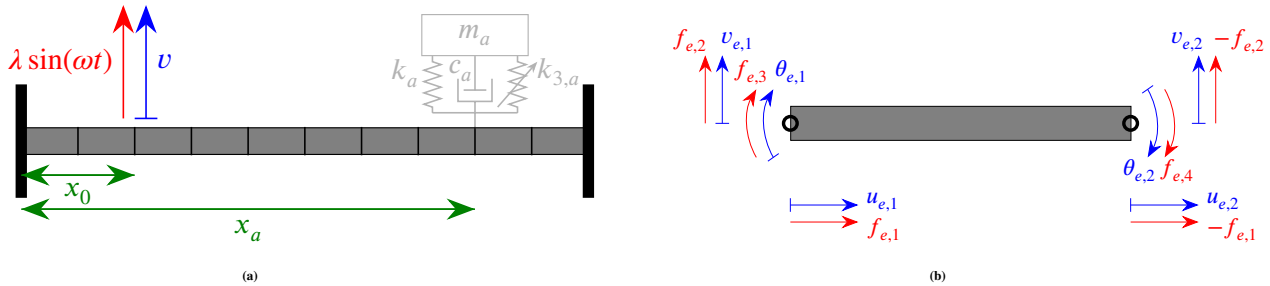

Figure 10 Schematic representation of the doubly clamped beam (a) and of a beam element (b); quantities in blue and red denote generalized DoFs and loadings, respectively.

Young's modulus	Density	Length	Width	Thickness	x_0	x_a
210 GPa	7800 kg/m^3	500 mm	20 mm	1 mm	100 mm	400 mm

Table 1 Material and geometrical parameters of the doubly clamped beam.

A finite element formalism as proposed in[60] was used to model the beam. Each element has six DoFs (the axial and transversal displacements and the rotations of both nodes), as depicted in Figure 10b, which are assumed to be identified from the global DoFs with a localization (Boolean) matrix $\mathbf{L}_e$, i.e.,

$$\left[u_{e,1}\ v_{e,1}\ \theta_{e,1}\ u_{e,2}\ v_{e,2}\ \theta_{e,2}\right]^T = \mathbf{L}_e\mathbf{x}. \tag{81}$$

Linear and cubic shape functions are adopted for the axial and transversal displacements, respectively. To each element are associated four nonlinear forces, representing the axial and transversal forces across the element, and the two moments at the

nodes, as shown in Figure 10b. The quantities for the formalism of Equation (59) for the nonlinear forces for each element are

$$\left[\mathbf{b}_{e,1}\ \mathbf{b}_{e,2}\ \mathbf{b}_{e,3}\ \mathbf{b}_{e,4}\right] = \mathbf{L}_e^T \begin{bmatrix} 1 & 0 & 0 & 0 \\ 0 & 1 & 0 & 0 \\ -1 & 0 & 0 & 0 \\ 0 & -1 & 0 & 0 \\ 0 & 0 & 1 & 0 \\ 0 & 0 & 0 & 1 \end{bmatrix}, \qquad \mathbf{C}_{e,i} = \mathbf{L}_e,\ i = 1, 2, 3, 4. \tag{82}$$

The expressions of the nonlinear forces are given in[60] (Equation (A.16), lines 1, 2, 3 and 6 therein). The Jacobian and the two-mode vector products of the Hessian were symbolically computed in Wolfram Mathematica. The resulting expressions were then exported to an in-home MATLAB code. Owing to the rather long character of these expressions, they are not reported here.

The beam was discretized with 10 elements, thereby yielding a system with 27 DoFs (accounting for the boundary conditions) for the bare beam, plus one for the absorber. Proportional modal damping of 0.5% for the first two bending modes was added to the structure.

6.3.2 | Uncontrolled beam response

Figure 11a depicts the NFR of the transversal DoF collocated with the forcing evaluated at $\lambda = 0.02$ N, as well as the results from the phase resonance and extremum tracking procedures. Both approaches yield indistinguishably accurate results to characterize the amplitude resonance of the structure. For a better assessment of the accuracy, Figure 11b compares the phase resonance and extremum tracking approaches through the relative error of the former with respect to the latter. In this case, phase resonance appears to be an excellent substitute for extremum tracking, given its overall small error of the order of 0.025%. The small dip in the error around $\lambda = 0.01$ N occurs near a weak 5:1 modal interaction of the first and third bending modes.

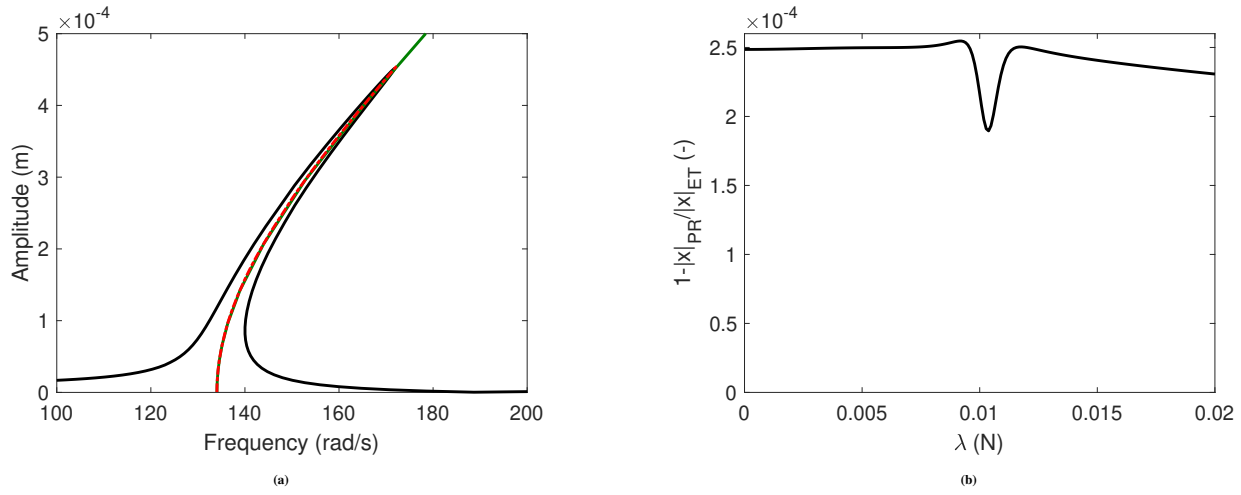

Figure 11 NFR of the doubly clamped beam at $\lambda = 0.02$ N (—), phase resonance (—) and extremum tracking (—) (a); relative error of the phase resonance amplitude x_{PR} with respect to the extremum x_{ET} (b).

To illustrate the merit of the different tracking approaches, Table 2 gathers their computational times. Similarly to[30], all CPU times are normalized with respect to the average CPU time for a step of the NFR computation. For a fair assessment of the benefits of the proposed AFT approach for second derivatives, a comparison is also made where the derivatives of g_p are evaluated using finite differences (whereas the N_z first lines of Equation (21) are computed with the standard analytical sensitivity formulas). To do so, Equation (46) is used, but the derivatives of $\tilde{\mathbf{J}}$ are evaluated using forward finite differences, similarly to what was done in[29].

Phase resonance appears to be largely advantageous in this case, in accordance with the rationale behind[39]. Not only is one continuation step almost as cheap to compute as an NFR computation, but the method can also take large steps within the adaptive scheme. The extremum tracking procedure is more computationally expensive, owing to the need for second derivative

Method	NFR	PR	ET (AFT)	ET (FD)
Normalized average CPU time per step	1	1.17	5.68	349.29
Continuation steps	195	66	100	104
Total normalized CPU time	195	77.53	567.78	36326.59

Table 2 Computational cost of the different methods used to compute the response of the doubly clamped beam (PR stands for phase resonance, ET for extrema tracking, and FD for finite differences).

evaluations. Moreover, the adaptation scheme imposes smaller steps. These two aspects result in a total computational time about seven times larger than the phase resonance approach for this example. Nevertheless, substantial savings are obtained thanks to the proposed AFT procedure since the approach using finite differences takes a much longer time per step (by a factor of about 60).

6.3.3 | Controlled beam response

Phase resonance may not always be suitable to characterize amplitude resonances. As an illustration, a case where the beam is equipped with an NLTVA with a cubic spring to mitigate its vibration amplitude around the first resonance is considered[10]. The mass of the absorber was selected to be 5% of that of its host. The parameters of the absorber were then tuned following the approach in[61] (i.e., the linear parameters were first optimized numerically, and the coefficient of the cubic spring was tuned based on a perturbation method). The resulting design features two peaks of equal amplitude in linear regimes of motion, much lower that of the uncontrolled host's resonance. The nonlinearity of the absorber aims to enforce this property for nonlinear regimes of motion as well[10].

As shall be shown, the direct application of the approach in[61] improves performance, albeit not optimally in nonlinear regimes of motion. This comes from the presence of quadratic nonlinearities and in particular from the effect of mid-plane stretching on bending dynamics. The presence of quadratic nonlinearities invalidates the assumption of[61] that there are only odd nonlinearities in the system, explaining why a direct application of the method fails to provide an optimal design.

It is nonetheless possible to obtain an optimal tuning if the membrane effects are correctly accounted for through an effective value of the cubic nonlinear bending stiffness. To obtain this, the implicit condensation method was used[62]. The first four undamped modes of the controlled structure (which are all bending modes) were retained. Associated external static modal loadings were then applied to the structure. The resulting nonlinear forces were fitted with quadratic and cubic monomials in the retained modal coordinates. The external modal loadings amplitudes were selected so as to result in a maximum static displacement of the order of the thickness of the beam. Because the beam is straight, the effective quadratic nonlinearities should theoretically be zero and were indeed negligible in front of the effective cubic ones. This allowed to construct a new expression of the nonlinear forces containing only effective cubic nonlinearities wherein the nonlinear membrane strain effects were correctly accounted for. This effective nonlinearity was then used to tune the absorber based on the method in[61]. The resulting parameters are given in Table 3.

m_a	c_a	k_a	$k_{3,a}$
0.0039 kg	0.09 kg/s	68.3503 N/m	1.3764×10^7 N/m^3

Table 3 Parameters of the NLTVA.

Figure 12 depicts the NFR of the controlled beam in quasi-linear ($\lambda = 0.03$ N) and strongly nonlinear ($\lambda = 0.15$ N) regimes of motion. As expected, the former features two peaks of (almost) equal amplitude. In the strongly nonlinear regime of motion, the merging of an isola with the rightmost peak leads to a substantial increase of the maximum amplitude, as can be seen in Figure 12a. Figure 12b shows that no specific phase relation can be used to approximate the loci of resonant peaks. This result is to be expected, given the close frequencies and high modal damping of the two resonances of the controlled system.

Figure 13a presents the NFRs of the system at multiple forcing amplitudes, up to $\lambda = 0.15$, along with the results of the proposed tracking method. Once again, the peaks are accurately tracked, which gives a direct assessment of the absorber's performance. The birth and merging with the rightmost peak of the isola is also highlighted by the peaks locus.

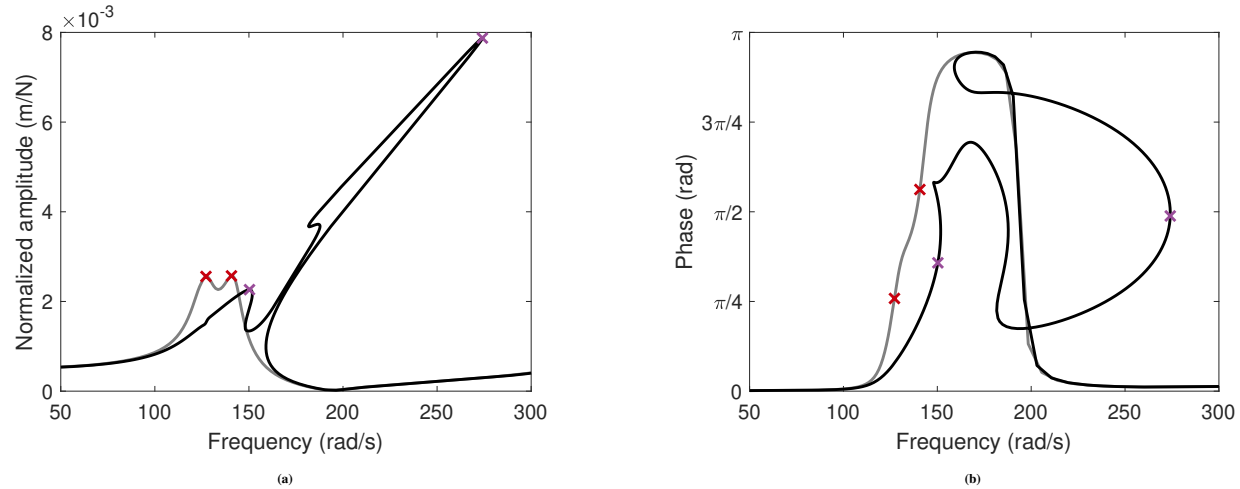

Figure 12 Normalized NFRs of the controlled beam at $\lambda = 0.03$ (—: NFR, ×: amplitude peaks) and $\lambda = 0.15$ (—: NFR, ×: amplitude peaks): normalized multi-harmonic amplitude (a), and phase of the first harmonic (b).

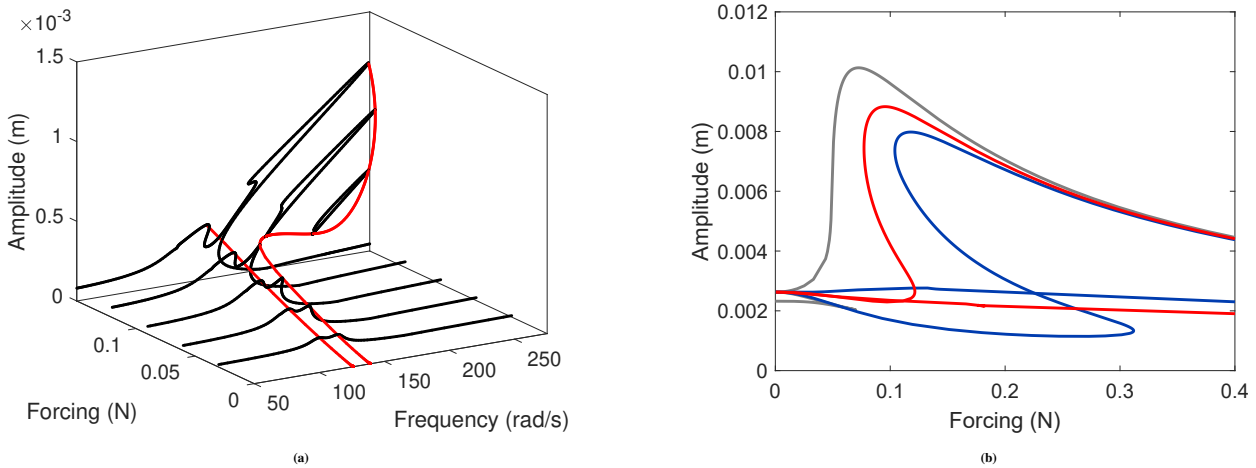

Figure 13 Set of NFRs of the controlled beam (—) and multi-amplitude extrema (—) (a) and loci of extrema of different designs: linear absorber (—), optimal NLTVA (—) and NLTVA tuned ignoring nonlinear membrane effects (—) (b).

Figure 13b presents the tracked extrema in the (λ, a) plane. The optimal design is compared to two other cases, namely a linear absorber ($k_{3,a}$=0) and a NLTVA tuned ignoring the nonlinear membrane effects on bending ($k_{3,a} = 1.9127 \times 10^7$ N/m^3). The proposed method allows for a quick performance assessment of different designs. It can be seen that the optimal design leads to the lowest maximum amplitude up to $\lambda \approx 0.1$ N, and this (near-)optimal character can be recognized by the (near-)tangency of the two branches of the peak locus at $\lambda = 0$ N, indicating that the amplitudes of the peaks remain (nearly) equal in spite of the nonlinearity of the host [10,61]. The dynamics of the system around the controlled resonance qualitatively resemble those of a single-DoF host. More detailed analyses of the dynamics of this system can be found in [10,32,33].

7 | CONCLUSION

This work proposed a numerical method to track the amplitude extrema of nonlinear frequency responses. Semi-analytical procedures were reviewed to compute the maximum amplitude of a multi-harmonic Fourier series. These results were then

incorporated into a continuation procedure tracking the amplitude extrema. Combined with the use of bordered matrices and an alternating frequency-time procedure, the proposed method was shown to be accurate and efficient through various examples.

Compared with its state-of-the-art counterparts, namely, single-harmonic amplitude extrema tracking [36,38] and phase resonance tracking [39], the proposed method is able to follow accurately the amplitude extrema of the multi-harmonic balance method results. Phase resonance is an excellent method to characterize the primary resonances of lightly-damped systems, but can be less accurate when applied to systems with moderate damping and/or closely-spaced resonant frequencies. The proposed method comes in as an adequate, albeit more computationally expensive substitute. It can also detect isolas similarly to fold bifurcation tracking procedures [29,33] for a similar computational cost while not requiring a fold bifurcation to initiate the continuation.

The proposed AFT procedure for second derivatives may also find direct applications for bifurcation tracking [29,30]. Its two main limitations come from smoothness requirements on the functional forms that are necessary to compute second derivatives and its intrusive character. Although a large class of commonly-used nonlinearities do not respect the smoothness conditions, this issue can be circumvented with regularization. Alternatively, the ideas proposed in [47,63] could be extended to/exploited for the case of second derivatives. The intrusive character of the method will generally prevent its use with commercial codes, but this issue could be mitigated using reduction or hyper-reduction methods [64].

The method could also be generalized in multiple ways. For instance, the extrema of more general quantities than DoFs can be tracked (such as nonlinear forces or energy quantities), as long as their Fourier series (and sensitivities) are available. Considering a continuation parameter λ other than the external forcing could also constitute an interesting tool to evaluate different designs. Finally, the ideas developed in this manuscript could be adapted for other methods than HB. Shooting-based procedures could rely on the integration of second-order variational equations [48] (or some adaptation of it), whereas collocation-based procedures would likely follow similar developments as the HB-based method.

ACKNOWLEDGEMENTS

Ghislain Raze is a Postdoctoral Researcher of the Fonds de la Recherche Scientifique - FNRS which is gratefully acknowledged.

CONFLICT OF INTEREST STATEMENT

The authors declare no potential conflict of interest. The authors do not possess any financial conflicts of interest to disclose.

DATA AVAILABILITY STATEMENT

The data that support the findings of this study are available from the corresponding author upon reasonable request.

□

APPENDIX

A ALTERNATIVE FORMULATION FOR EXTREMUM TRACKING

This appendix presents an alternative formulation for an extremum tracking procedure based on the method proposed by Petrov [36]. It will be shown that this formulation leads to ill numerical conditioning when the extrema are close to fold bifurcations.

A.1 Extrema tracking using a horizontal tangent equation

An extremum of the NFR amplitude is simply a point whose total derivative of the amplitude with respect to ω (with fixed λ) is zero. Hence, the following necessary condition must be met to characterize a peak of the NFR

$$\frac{da}{d\omega} = \frac{d}{d\omega}\left(\left|\mathbf{Q}(\tau_{\max}(\mathbf{z}))\mathbf{B}_u\mathbf{z}\right|\right) = \operatorname{sign}\left(\mathbf{Q}(\tau_{\max}(\mathbf{z}))\mathbf{B}_u\mathbf{z}\right)\mathbf{Q}(\tau_{\max}(\mathbf{z}))\mathbf{B}_u\frac{d\mathbf{z}}{d\omega} = 0, \tag{A1}$$

where Equation (13) has been used. This condition features the total derivative of $\mathbf{z}$ with respect to ω (with fixed λ), which is obtained by differentiating Equation (4), yielding

$$\left(\mathbf{A}(\omega)+\frac{\partial \mathbf{b}}{\partial \mathbf{z}}\right)\frac{d\mathbf{z}}{d\omega}+\frac{\partial \mathbf{A}(\omega)}{\partial \omega}\mathbf{z}+\frac{\partial \mathbf{b}}{\partial \omega}=\mathbf{0}, \tag{A2}$$

that is, if $\mathbf{A}(\omega)+\partial\mathbf{b}/\partial\mathbf{z}$ is nonsingular,

$$\frac{d\mathbf{z}}{d\omega}:=\mathbf{z}_{\omega}=-\left(\mathbf{A}(\omega)+\frac{\partial \mathbf{b}}{\partial \mathbf{z}}\right)^{-1}\left(\frac{\partial \mathbf{A}(\omega)}{\partial \omega}\mathbf{z}+\frac{\partial \mathbf{b}}{\partial \omega}\right). \tag{A3}$$

The minimally augmented set of equations that characterize a peak of the NFR amplitude is thus given by combining Equation (4) with the horizontal tangent requirement in Equation (A1) as

$$\begin{cases}\mathbf{A}(\omega)\mathbf{z}+\mathbf{b}(\omega,\mathbf{z})-\lambda\mathbf{b}_{\text{ext}}=\mathbf{0}\\ \text{sign}\left(\mathbf{Q}(\tau_{\max}(\mathbf{z}))\mathbf{B}_u\mathbf{z}\right)\mathbf{Q}(\tau_{\max}(\mathbf{z}))\mathbf{B}_u\mathbf{z}_{\omega}(\mathbf{z},\omega)=0\end{cases}. \tag{A4}$$

This set of N_z+1 equations is to be solved for N_z+2 unknowns ($\mathbf{z}$, ω and λ). A classical continuation procedure can be used.

A.2 Singularity issues

$\mathbf{z}_{\omega}$ and its derivatives can be obtained using Equation (A3) provided that the matrix $\mathbf{A}(\omega)+\partial\mathbf{b}/\partial\mathbf{z}$ is not singular. Two notable exceptions to this requirement are fold and branch point bifurcations.

At a fold bifurcation, the system in Equation (A2) does not have a solution because[3]

$$\frac{\partial \mathbf{A}(\omega)}{\partial \omega}\mathbf{z}+\frac{\partial \mathbf{b}}{\partial \omega}\notin \text{range}\left(\mathbf{A}(\omega)+\frac{\partial \mathbf{b}}{\partial \mathbf{z}}\right). \tag{A5}$$

This issue comes from the fact that a point on the (ω,a) graph of the NFR should at the same time feature a vertical and horizontal tangent. The only cases which somewhat conciliate these conflicting requirements occur when the tangent is undefined, e.g., when the curve forms a cusp, or at the birth of an isola. NFR curves in situations close to these degenerate cases feature large variations of the tangent orientation for small variations of the parameters. When the extrema are close to fold bifurcations, the method proposed in[36] is thus expected to be ill-conditioned. We note that fold bifurcations can occur close to amplitude maxima, especially in lightly-damped geometrically nonlinear structures, which may explain why this method was found to be rather inefficient in[39].

A.3 Illustration with the NLTVA

The example of an NLTVA controlling a Duffing oscillator with a mass ratio of 5% is taken from[10]. A figure in appearance in all points similar to Figure 13 can be obtained with the multi-harmonic generalization of[36]. However, looking closely at the steps taken by the continuation procedure, a discrepancy between the two formulations can be observed. Figure A1a plots the evolution of λ (the forcing amplitude) of the extremum tracking procedure when the rightmost peak is tracked and compares it for the different formulations. The method based on the formulation of[38] reaches the final value ($\lambda=0.25$) in about four times less continuation iterations than that of[36].

The continuation procedures were run using finite differences to compute the derivatives as well. As can be seen in Figure A1a, while there is no observable change for the continuation procedure with finite differences for the formulation of[38], there is a clear difference for that of[36]. The continuation procedure with finite differences does not even terminate at the correct final value of λ because the adaptive continuation step becomes too small, which results in an abortion of the procedure when it reaches the maximum number of continuation steps (in this case 500, although the last 200 steps were not plotted because they feature no significant evolution).

Figure A1b shows the condition number of the tangent prediction matrix used in the predictor-corrector scheme. This confirms that the stagnation of the continuation procedure occurs when the system is ill-conditioned. We note that this stagnation phenomenon happens close to the extremal values of λ, which correspond to the merging and birth of the isola. In these situations, the NFR features a cusp and reduces to a single point, respectively, thereby corresponding to the situations described previously. This example thus illustrates the ill conditioning of a method based on that of[36] close to fold bifurcations, and the more robust character of that of[38].

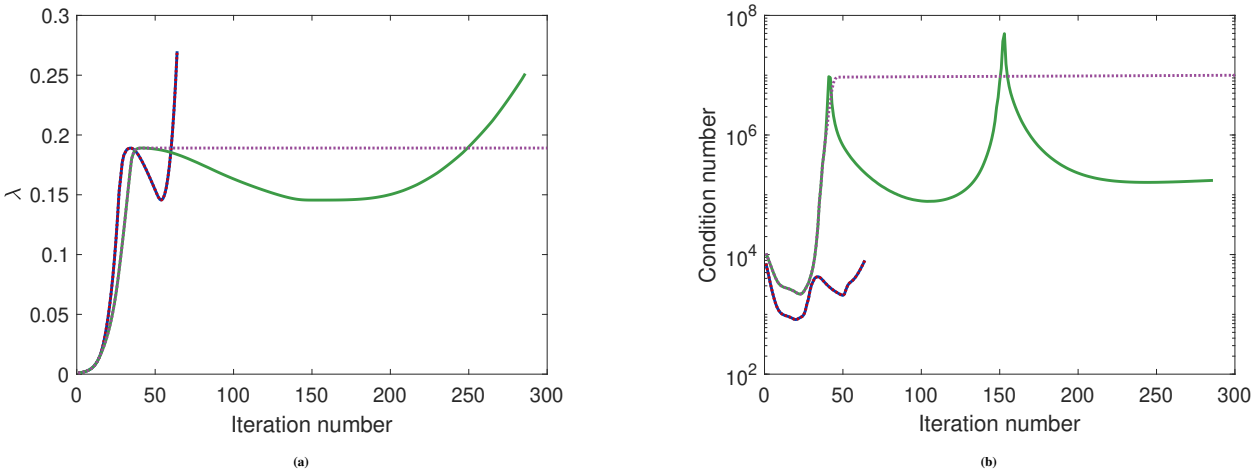

Figure A1 Evolution of the continuation procedure using the formulation of[38] with analytical derivatives (—) or finite differences (—) and the formulation of[36] with analytical derivatives (—) or finite differences (—): forcing amplitude (a) and condition number of the tangent prediction matrix (b).

B DIFFERENTIABILITY OF THE AMPLITUDE OF FOURIER SERIES WITH ODD TERMS

A Fourier series with only odd terms can be written as

$$u(\tau) = \sum_{k=1}^{\llcorner (N_h+1)/2 \lrcorner} \left(z_{s,2k-1} \sin((2k-1)\tau) + z_{c,2k-1} \cos((2k-1)\tau) \right). \tag{B6}$$

Since in this case $u(\tau) = -u(\tau + \pi)$, if a value τ_{max} is found for an extremum, another amplitude extremum necessarily occurs at $\tau_{max} + \pi$. Odd Fourier series thus always have at least two amplitude extrema. It is possible to show that this multiplicity of extrema is an issue for the derivatives of a with respect to the even harmonic coefficients, but not for the odd ones.

To show this, we investigate if the derivatives differ when they are evaluated at $\tau_{max,1}$ or $\tau_{max,2} = \tau_{max,1} + \pi$. We first note that since the second time derivative of u is also an odd Fourier series, $u''(\tau_{max,1}) = -u''(\tau_{max,1} + \pi) = -u''(\tau_{max,2})$.

Using Equation (57), the derivative of τ_{max} with respect to an odd cosine coefficient

$$\frac{\partial \tau_{max,1}}{\partial z_{c,2k-1}} = \frac{(2k-1)\sin((2k-1)\tau_{max,1})}{u''(\tau_{max,1})} = \frac{-(2k-1)\sin((2k-1)\tau_{max,2})}{-u''(\tau_{max,2})} = \frac{\partial \tau_{max,2}}{\partial z_{c,2k-1}} \tag{B7}$$

is identical whether it is evaluated at $\tau_{max,1}$ or $\tau_{max,2}$. The same property holds for a derivative with respect to an odd sine coefficient. However, the derivatives with respect to an even cosine coefficient are

$$\frac{\partial \tau_{max,1}}{\partial z_{c,2k}} = \frac{2k\sin(2k\tau_{max,1})}{u''(\tau_{max,1})} = \frac{2k\sin(2k\tau_{max,2})}{-u''(\tau_{max,2})} = -\frac{\partial \tau_{max,2}}{\partial z_{c,2k}}. \tag{B8}$$

This non-uniqueness of the derivative of τ_{max} results from the nonsmooth character of the amplitude. The same issue occurs for derivatives with respect to an even sine coefficient. The converse can also be shown, that even Fourier series are nonsmooth when derivatives with respect to odd harmonic coefficients are considered, but is not detailed here.

As a simple illustration, the amplitude of $u(\tau) = z_{c,0} + z_{c,1}\cos(\tau)$ is $a = |z_{c,0}| + |z_{c,1}|$, which is nonsmooth at $z_{c,0} = 0$ (and at $z_{c,1} = 0$). However, when $z_{c,0} \neq 0$ and $z_{c,1} \neq 0$, there is only one amplitude maximum for the Fourier series, and the amplitude is a smooth function of its arguments.

References

1. Guckenheimer J, Holmes P. *Nonlinear Oscillations, Dynamical Systems, and Bifurcations of Vector Fields*. 42 of *Applied Mathematical Sciences*. New York, NY: Springer New York . 1983

2. Nayfeh AH, Mook DT. *Nonlinear Oscillations*. Wiley . 1995

3. Seydel R. *Practical Bifurcation and Stability Analysis*. 5 of *Interdisciplinary Applied Mathematics*. New York, NY: Springer New York . 2010

4. Krack M, Gross J. *Harmonic Balance for Nonlinear Vibration Problems*. Mathematical EngineeringCham: Springer International Publishing . 2019

5. Worden K, Tomlinson GR. *Nonlinearity in Structural Dynamics*. IOP Publishing Ltd . 2001

6. Vakakis AF, Gendelman OV, Bergman LA, McFarland DM, Kerschen G, Lee YS. *Nonlinear Targeted Energy Transfer in Mechanical and Structural Systems*. 156 of *Solid Mechanics and Its Applications*. Dordrecht: Springer Netherlands . 2009

7. Dekemele K, De Keyser R, Loccufier M. Performance measures for targeted energy transfer and resonance capture cascading in nonlinear energy sinks. *Nonlinear Dyn.* 2018; 93(2): 259–284. doi: 10.1007/s11071-018-4190-5

8. Oueini SS, Nayfeh AH. Analysis and Application of a Nonlinear Vibration Absorber. *J. Vib. Control* 2000; 6(7): 999–1016. doi: 10.1177/107754630000600703

9. Shami ZA, Giraud-Audine C, Thomas O. A nonlinear piezoelectric shunt absorber with a 2:1 internal resonance: Theory. *Mech. Syst. Signal Process.* 2022; 170(December 2021): 108768. doi: 10.1016/j.ymssp.2021.108768

10. Habib G, Detroux T, Viguié R, Kerschen G. Nonlinear generalization of Den Hartog's equal-peak method. *Mechanical Systems and Signal Processing* 2015; 52-53(1): 17–28. doi: 10.1016/j.ymssp.2014.08.009

11. Lossouarn B, Deü JF, Kerschen G. A fully passive nonlinear piezoelectric vibration absorber. *Philos. Trans. R. Soc. A Math. Phys. Eng. Sci.* 2018; 376(2127): 20170142. doi: 10.1098/rsta.2017.0142

12. Krack M, Salles L, Thouverez F. Vibration Prediction of Bladed Disks Coupled by Friction Joints. *Arch. Comput. Methods Eng.* 2017; 24(3): 589–636. doi: 10.1007/s11831-016-9183-2

13. Denimal E, El Haddad F, Wong C, Salles L. Topological Optimization of Under-Platform Dampers With Moving Morphable Components and Global Optimization Algorithm for Nonlinear Frequency Response. *J. Eng. Gas Turbines Power* 2021; 143(2). doi: 10.1115/1.4049666

14. Li H, Touzé C, Pelat A, Gautier F, Kong X. A vibro-impact acoustic black hole for passive damping of flexural beam vibrations. *J. Sound Vib.* 2019; 450: 28–46. doi: 10.1016/j.jsv.2019.03.004

15. Chabrier R, Chevallier G, Foltête E, Sadoulet-Reboul E. Experimental investigations of a vibro-impact absorber attached to a continuous structure. *Mech. Syst. Signal Process.* 2022; 180(February): 109382. doi: 10.1016/j.ymssp.2022.109382

16. Theurich T, Krack M. Experimental validation of impact energy scattering as concept for mitigating resonant vibrations.. *J. Struct. Dyn.* 2023: 1–23. doi: 10.25518/2684-6500.126

17. Agarwal M, Chandorkar SA, Candler RN, et al. Optimal drive condition for nonlinearity reduction in electrostatic microresonators. *Appl. Phys. Lett.* 2006; 89(21): 214105. doi: 10.1063/1.2388886

18. Dou S, Strachan BS, Shaw SW, Jensen JS. Structural optimization for nonlinear dynamic response. *Philos. Trans. R. Soc. A Math. Phys. Eng. Sci.* 2015; 373(2051): 20140408. doi: 10.1098/rsta.2014.0408

19. Habib G, Kerschen G. Linearization of nonlinear resonances: Isochronicity and force-displacement proportionality. *J. Sound Vib.* 2019; 457: 227–239. doi: 10.1016/j.jsv.2019.06.007

20. Detroux T, Noël JP, Kerschen G. Tailoring the resonances of nonlinear mechanical systems. *Nonlinear Dyn.* 2020. doi: 10.1007/s11071-020-06002-w

21. Hermann M, Ullrich K. RWPKV: A software package for continuation and bifurcation problems in two-point boundary value problems. *Appl. Math. Lett.* 1992; 5(2): 57–61. doi: 10.1016/0893-9659(92)90112-M

22. A Collocation Solver for Mixed Order Systems of Boundary Value Problems. *Math. Comput.* 1979; 33(146): 659. doi: 10.2307/2006301

23. Doedel E, Keller HB, Kernevez JP. Numerical analysis and control of bifurcation problems (I): bifurcations in finite dimensions. *Int. J. Bifurc. Chaos* 1991; 01(03): 493–520. doi: 10.1142/S0218127491000397

24. Dhooge A, Govaerts W, Kuznetsov YA. MATCONT: A MATLAB Package for Numerical Bifurcation Analysis of ODEs. *ACM Trans. Math. Softw.* 2003; 29(2): 141–164. doi: 10.1145/779359.779362

25. Dankowicz H, Schilder F. An Extended Continuation Problem for Bifurcation Analysis in the Presence of Constraints. *J. Comput. Nonlinear Dyn.* 2011; 6(3). doi: 10.1115/1.4002684

26. Cochelin B, Vergez C. A high order purely frequency-based harmonic balance formulation for continuation of periodic solutions. *J. Sound Vib.* 2009; 324(1-2): 243–262. doi: 10.1016/j.jsv.2009.01.054

27. Slater JC. Mousai: An Open Source Harmonic Balance Solver for Nonlinear Systems. 13th ASME Dayton Engineering Sciences Symposium; 2017. Dayton, OH.

28. Salinger AG, Burroughs EA, Pawlowski RP, Phipps ET, Romero LA. Bifurcation tracking algorithms and software for large scale applications. In: . 15. 2006 (pp. 319–336)

29. Detroux T, Renson L, Masset L, Kerschen G. The harmonic balance method for bifurcation analysis of large-scale nonlinear mechanical systems. *Computer Methods in Applied Mechanics and Engineering* 2015; 296: 18–38. doi: 10.1016/j.cma.2015.07.017

30. Xie L, Baguet S, Prabel B, Dufour R. Bifurcation tracking by Harmonic Balance Method for performance tuning of nonlinear dynamical systems. *Mechanical Systems and Signal Processing* 2017; 88(September 2016): 445–461. doi: 10.1016/j.ymssp.2016.09.037

31. Quaegebeur S, Di Palma N, Chouvion B, Thouverez F. Exploiting internal resonances in nonlinear structures with cyclic symmetry as a mean of passive vibration control. *Mech. Syst. Signal Process.* 2022; 178(December 2021): 109232. doi: 10.1016/j.ymssp.2022.109232

32. Detroux T, Habib G, Masset L, Kerschen G. Performance, robustness and sensitivity analysis of the nonlinear tuned vibration absorber. *Mech. Syst. Signal Process.* 2015; 60-61: 799–809. doi: 10.1016/j.ymssp.2015.01.035

33. Grenat C, Baguet S, Lamarque CH, Dufour R. A multi-parametric recursive continuation method for nonlinear dynamical systems. *Mech. Syst. Signal Process.* 2019; 127: 276–289. doi: 10.1016/j.ymssp.2019.03.011

34. Boyd S, Balakrishnan V. A regularity result for the singular values of a transfer matrix and a quadratically convergent algorithm for computing its L/sub infinity /-norm. In: IEEE; 1990: 954–955

35. Bruinsma N, Steinbuch M. A fast algorithm to compute the H∞ norm of a transfer function matrix. *Syst. Control Lett.* 1990; 14(4): 287–293. doi: 10.1016/0167-6911(90)90049-Z

36. Petrov EP. Direct Parametric Analysis of Resonance Regimes for Nonlinear Vibrations of Bladed Disks. *J. Turbomach.* 2007; 129(3): 495–502. doi: 10.1115/1.2720487

37. Liao H, Sun W. A new method for predicting the maximum vibration amplitude of periodic solution of non-linear system. *Nonlinear Dyn.* 2013; 71(3): 569–582. doi: 10.1007/s11071-012-0682-x

38. Renault A, Thomas O, Mahé H. Numerical antiresonance continuation of structural systems. *Mechanical Systems and Signal Processing* 2019; 116: 963–984. doi: 10.1016/j.ymssp.2018.07.005

39. Förster A, Krack M. An efficient method for approximating resonance curves of weakly-damped nonlinear mechanical systems. *Comput. Struct.* 2016; 169: 81–90. doi: 10.1016/j.compstruc.2016.03.003

40. Peter S, Leine RI. Excitation power quantities in phase resonance testing of nonlinear systems with phase-locked-loop excitation. *Mech. Syst. Signal Process.* 2017; 96: 139–158. doi: 10.1016/j.ymssp.2017.04.011

41. Denis V, Jossic M, Giraud-Audine C, Chomette B, Renault A, Thomas O. Identification of nonlinear modes using phase-locked-loop experimental continuation and normal form. *Mech. Syst. Signal Process.* 2018; 106: 430–452. doi: 10.1016/j.ymssp.2018.01.014

42. Scheel M, Peter S, Leine RI, Krack M. A phase resonance approach for modal testing of structures with nonlinear dissipation. *J. Sound Vib.* 2018; 435: 56–73. doi: 10.1016/j.jsv.2018.07.010

43. Cenedese M, Haller G. How do conservative backbone curves perturb into forced responses? A Melnikov function analysis. *Proc. R. Soc. A Math. Phys. Eng. Sci.* 2020; 476(2234): 20190494. doi: 10.1098/rspa.2019.0494

44. Volvert M, Kerschen G. Phase resonance nonlinear modes of mechanical systems. *J. Sound Vib.* 2021; 511(July): 116355. doi: 10.1016/j.jsv.2021.116355

45. Volvert M, Kerschen G. Resonant phase lags of a Duffing oscillator. *Int. J. Non. Linear. Mech.* 2022; 146(July): 104150. doi: 10.1016/j.ijnonlinmec.2022.104150

46. Govaerts WJF. *Numerical Methods for Bifurcations of Dynamical Equilibria*. Society for Industrial and Applied Mathematics . 2000

47. Krack M, Panning-von Scheidt L, Wallaschek J. A high-order harmonic balance method for systems with distinct states. *J. Sound Vib.* 2013; 332(21): 5476–5488. doi: 10.1016/j.jsv.2013.04.048

48. Rein H, Tamayo D. Second-order variational equations for N -body simulations. *Mon. Not. R. Astron. Soc.* 2016; 459(3): 2275–2285. doi: 10.1093/mnras/stw644

49. Neidinger RD. Introduction to Automatic Differentiation and MATLAB Object-Oriented Programming. *SIAM Rev.* 2010; 52(3): 545–563. doi: 10.1137/080743627

50. Cameron TM, Griffin JH. An Alternating Frequency/Time Domain Method for Calculating the Steady-State Response of Nonlinear Dynamic Systems. *Journal of Applied Mechanics* 1989; 56(1): 149. doi: 10.1115/1.3176036

51. Boyd JP. Computing the zeros, maxima and inflection points of Chebyshev, Legendre and Fourier series: solving transcendental equations by spectral interpolation and polynomial rootfinding. *J. Eng. Math.* 2007; 56(3): 203–219. doi: 10.1007/s10665-006-9087-5

52. Manocha D. Solving systems of polynomial equations. *IEEE Comput. Graph. Appl.* 1994; 14(2): 46–55. doi: 10.1109/38.267470

53. Woiwode L, Balaji NN, Kappauf J, et al. Comparison of two algorithms for Harmonic Balance and path continuation. *Mech. Syst. Signal Process.* 2020; 136: 106503. doi: 10.1016/j.ymssp.2019.106503

54. Ju R, Fan W, Zhu WD. Comparison Between the Incremental Harmonic Balance Method and Alternating Frequency/Time-Domain Method. *J. Vib. Acoust.* 2021; 143(2): 1–7. doi: 10.1115/1.4048173

55. Bader BW, Kolda TG. Efficient MATLAB Computations with Sparse and Factored Tensors. *SIAM J. Sci. Comput.* 2008; 30(1): 205–231. doi: 10.1137/060676489

56. Petrov EP. Sensitivity Analysis of Nonlinear Forced Response for Bladed Discs With Friction Contact Interfaces. In: . 5. ASMEDC; 2005: 483–494

57. Cox Jr S, Nadler Jr S. Supremum norm differentiability. *Comment. Math.* 1971; 15(1).

58. Fayezioghani A, Vandoren B, Sluys L. Performance-based step-length adaptation laws for path-following methods. *Comput. Struct.* 2019; 223: 106100. doi: 10.1016/j.compstruc.2019.07.009

59. Detroux T. *Performance and Robustness of Nonlinear Systems Using Bifurcation Analysis*. PhD thesis. University of Liège, 2016.

60. Lazarus A, Thomas O, Deü JF. Finite element reduced order models for nonlinear vibrations of piezoelectric layered beams with applications to NEMS. *Finite Elem. Anal. Des.* 2012; 49(1): 35–51. doi: 10.1016/j.finel.2011.08.019

61. Raze G, Kerschen G. Multimodal vibration damping of nonlinear structures using multiple nonlinear absorbers. *Int. J. Non. Linear. Mech.* 2020; 119: 103308. doi: 10.1016/j.ijnonlinmec.2019.103308

62. McEwan M, Wright J, Cooper J, Leung A. A combined modal/finite element analysis technique for the dynamic response of a non-linear beam to harmonic excitation. *J. Sound Vib.* 2001; 243(4): 601–624. doi: 10.1006/jsvi.2000.3434

63. Petrov EP, Ewins DJ. Analytical Formulation of Friction Interface Elements for Analysis of Nonlinear Multi-Harmonic Vibrations of Bladed Disks. *J. Turbomach.* 2003; 125(2): 364–371. doi: 10.1115/1.1539868

64. Jain S, Tiso P. Simulation-Free Hyper-Reduction for Geometrically Nonlinear Structural Dynamics: A Quadratic Manifold Lifting Approach. *J. Comput. Nonlinear Dyn.* 2018; 13(7): 1–12. doi: 10.1115/1.4040021